The *Caenorhabditis elegans* nephrocystins act as global modifiers of cilium structure

Andrew R. Jauregui,[1,2] Ken C.Q. Nguyen,[4] David H. Hall,[4] and Maureen M. Barr[1,3]

[1]Department of Genetics, Rutgers University, Piscataway, NJ 08854
[2]Laboratory of Genetics, and [3]School of Pharmacy, University of Wisconsin-Madison, Madison, WI 53705
[4]Center for *C. elegans* Anatomy, Department of Neuroscience, Albert Einstein College of Medicine, New York, NY 10461

Nephronophthisis (NPHP) is the most common genetic cause of end-stage renal disease in children and young adults. In *Chlamydomonas reinhardtii*, *Caenorhabditis elegans*, and mammals, the NPHP1 and NPHP4 gene products nephrocystin-1 and nephrocystin-4 localize to basal bodies or ciliary transition zones (TZs), but their function in this location remains unknown. We show here that loss of *C. elegans* NPHP-1 and NPHP-4 from TZs is tolerated in developing cilia but causes changes in localization of specific ciliary components and a broad range of subtle axonemal ultrastructural defects. In amphid channel cilia, *nphp-4* mutations cause B tubule defects that further disrupt intraflagellar transport (IFT). We propose that NPHP-1 and NPHP-4 act globally at the TZ to regulate ciliary access of the IFT machinery, axonemal structural components, and signaling molecules, and that perturbing this balance results in cell type–specific phenotypes.

Introduction

Nephronophthisis (NPHP) is a rare autosomal recessive tubulointerstitial nephropathy characterized by cystic kidneys and renal fibrosis. NPHP extrarenal manifestations may include retinal degeneration, situs inversus, and neurological disorders. Mutations in one of nine genes (*NPHP1-9*) account for ∼35% of all NPHP cases, which suggests that other disease-causing loci exist (Caridi at al., 2006; Arts et al., 2007; Attanasio et al., 2007; Delous et al., 2007; for review see Hildebrandt and Zhou, 2007; Otto et al., 2008). The NPHP gene products, the nephrocystins, have been localized to several regions of the cell including the cilium (Hildebrandt et al., 1997; Olbrich et al., 2003; Otto et al., 2003, 2005; Mollet et al., 2005; Sayer et al., 2006). Given that many cell types possess cilia, it is not surprising that NPHP presents with a variety of extrarenal pathologies that may correlate with ciliary dysfunction (Pazour and Rosenbaum, 2002).

Cilia are specialized microtubule-based organelles that function in motility or sensation. Nonmotile primary cilia are found on most nondividing vertebrate cells (Wheatley 1995). In general, primary cilia have a 9 + 0 axoneme (nine outer doublet microtubules with no central pair). In the kidney, primary cilia project from the apical surfaces of epithelial cells and act as flow mechanosensors (Praetorius and Spring, 2001, 2003). In the eye, connecting cilia regulate protein trafficking between inner and outer photoreceptor segments (Marszalek et al., 2000; Pazour et al., 2002). In the mammalian embryo, nodal cilia exhibit a unique rotary motion required for left–right asymmetry (McGrath et al., 2003). Defects in these types of cilia may result in polycystic kidneys, retinal degeneration, and situs inversus, respectively (Pazour and Rosenbaum, 2002). In humans, perturbation of cilia formation, maintenance, morphogenesis, or function may result in a "ciliopathy" (Badano et al., 2006).

The development of all cilia and flagella requires intraflagellar transport (IFT; Rosenbaum and Witman, 2002). IFT was first observed in the alga *Chlamydomonas reinhardtii* as a rapid bidirectional movement of particles along the flagellar length in a FLA10 kinesin-2–dependent manner (Kozminski et al., 1993, 1995). The IFT kinesin-2 motor consists of two different heterodimerized motor subunits and one accessory (KAP) subunit (Cole et al., 1993). The basic unicellular IFT machinery comprises heterotrimeric kinesin-2 and retrograde cytoplasmic dynein motors that move IFT particles and cargo to and from the distal tips of cilia. The IFT particle is composed of two subcomplexes (IFT-A and IFT-B) containing 16–18 polypeptides (Cole et al., 1998). In *C. reinhardtii* and the nematode *Caenorhabditis*

Correspondence to M.M. Barr: barr@biology.rutgers.edu

Abbreviations used in this paper: BBS, Bardet-Biedl syndrome; Dyf, dye filling defective; IFT, intraflagellar transport; NPHP, nephronophthisis; PKD, polycystic kidney disease; SynDyf, synthetic Dyf; TAM, tubulin-associated material; TEM, transmission EM; TRP, transient receptor potential; TRPP, TRP polycystin; TRPV, TRP vanilloid; TZ, transition zone.

The online version of this paper contains supplemental material.

The Journal of Cell Biology, Vol. 180, No. 5, March 10, 2008 973–988
http://www.jcb.org/cgi/doi/10.1083/jcb.200707090

elegans, defects in IFT motors or polypeptides result in flagellar and ciliary defects. In mice, a mutation in the IFT88 polypeptide Polaris or the IFT kinesin-2 motor KIF3A causes autosomal recessive polycystic kidney disease (PKD; Pazour et al., 2000; Lin et al., 2003). In humans, IFT80 polypeptide mutations result in the ciliopathy Jeune asphyxiating thoracic dystropy (Beales et al., 2007).

C. elegans is a powerful model system to study ciliogenesis and human ciliopathies (Scholey et al., 2004; Barr, 2005; Badano et al., 2006). In the worm, IFT builds and maintains cilia on dendritic endings of sensory neurons. The amphids, a pair of lateral sensilla in the head, are the principal sensory organs of nematodes. Amphid channel cilia are ~7 μm in length and can be divided into three distinct segments (Ward et al., 1975; Perkins et al., 1986). The transition zone (TZ) is a modified basal body and the place where IFT proteins accumulate for transport into the axoneme. The axoneme has middle and distal segments, consisting of nine doublet (A tubule and B tubule) and nine singlet (A tubule only) microtubules, respectively. In addition to the amphids, four cuticular sensilla (cephalic, inner/outer labial quadrant, and outer labial lateral) are found in the head and the phasmid sensilla are located in the tail (Ward et al., 1975; Ware et al., 1975; Hall and Russell, 1991). In the male, each cephalic sensillum contains an additional exposed ciliated neuron (CEM) and the tail possesses sensilla required for sexual behaviors (Sulston et al., 1980; Liu and Sternberg, 1995; Barr and Sternberg, 1999). These cilia exhibit diverse morphologies and sensory properties (Sulston et al., 1980; Perkins et al., 1986; Bargmann, 2006).

In *C. elegans* amphid channel cilia, the IFT machinery has been extensively studied using mutant analysis combined with in vivo time-lapse fluorescence imaging (Orozco et al., 1999; Blacque et al., 2004; Snow et al., 2004; Ou et al., 2005, 2007; Pan et al., 2006). The following model has emerged. Amphid and phasmid channel cilia possess two IFT kinesin-2 motors: heterotrimeric kinesin-II and homodimeric OSM-3 (Shakir et al., 1993; Signor et al., 1999). The slow kinesin-II and fast OSM-3 act cooperatively to build the middle segment, whereas OSM-3 acts alone to drive IFT in the distal segment (Snow et al., 2004). Consistent with in vivo velocity measurements, purified mixtures of kinesin-II and OSM-3 produce intermediate motility rates in vitro (Pan et al., 2006). The Bardet-Biedl syndrome (BBS) proteins have been proposed to stabilize the association of the two kinesin-2 motors with their associated IFT subcomplexes (Ou et al., 2005, 2007). In a *bbs-1*, *bbs-7*, or *bbs-8* mutant background, IFT-A moves at the slow kinesin-II rate, whereas IFT-B moves at the fast OSM-3 rate. However, in a kinesin-II;*bbs* double mutant, IFT-A moves with OSM-3 and, likewise, in an *osm-3;bbs* double mutant, IFT-B moves with kinesin-II, which suggests that kinesin-II and OSM-3 mechanically compete for IFT-A and IFT-B in a BBS-dependent manner (Pan et al. 2006). Variations from the canonical slow, fast, and intermediate rates are observed in some mutant backgrounds, which indicates that there is an unappreciated complexity to IFT motor regulation (Burghoorn et al. 2007; Mukhopadhyay et al., 2007). Deviations observed from canonical rates in vivo may reflect changes in the normal molar ratio of active kinesin-II:OSM-3 bound to the IFT particles. Moreover, the basic IFT machinery is modified in a cell-specific manner to generate diversity in ciliary shape and function (Bae et al., 2006; Evans et al., 2006; Mukhopadhyay et al., 2007).

C. elegans nphp-1 and *nphp-4* orthologues are expressed in the ciliated sensory nervous system and are coexpressed with the *C. elegans* autosomal dominant PKD genes *lov-1/PKD1* and *pkd-2* (Jauregui and Barr 2005; Winkelbauer et al., 2005; Wolf et al., 2005). *nphp-1* and *nphp-4* deletion mutants form cilia as judged by lipophilic fluorescent dye filling and light microscopy, and are only slightly defective in several sensory behaviors. GFP-tagged NPHP-1 and NPHP-4 proteins localize to the ciliary TZ, with NPHP-1 requiring the presence of NPHP-4 for TZ localization (Winkelbauer et al., 2005). This TZ subcellular localization is evolutionarily conserved. Human nephrocystin-1 also localizes to the TZs of renal, respiratory, and photoreceptor connecting cilia (Schermer et al., 2005; Fliegauf et al., 2006). Moreover, both mammalian and *C. reinhardtii* nephrocystin-4 localize to ciliary basal bodies (Keller et al., 2005; Mollet et al., 2005). The TZ serves as a boundary between cytoplasmic and ciliary components and has been proposed to act as a "ciliary pore complex" (Rosenbaum and Witman, 2002). How the nephrocystins act at the TZ is not known.

In this paper, we address the functions of the nephrocystins in regulating ciliary receptor localization, ciliary shape, and ciliogenesis. *nphp-1* and *nphp-4* are not required for the ciliary localization of the transient receptor potential vanilloid (TRPV) channel OSM-9 (Colbert et al., 1997) or the TRP polycystin (TRPP) channel PKD-2 (Barr et al., 2001). Rather, *nphp-1* and *nphp-4* are important modulators of ciliary ultrastructure, with defects resulting in a broad phenotypic spectrum. Although not localizing to the axoneme, NPHP-1 and NPHP-4 indirectly regulate the velocity distributions of most IFT components examined. In addition, a subset of GFP-tagged IFT reporters (IFT52/OSM-6, OSM-3, BBS-7, and BBS-8) are mislocalized when NPHP-1 and NPHP-4 are absent from the TZ. In *nphp-4* animals, overexpression of OSM-6 results in abnormal association with kinesin-II in amphid middle segments and severe ciliogenic defects, likely because of sequestered IFT components at the TZ. We propose that the nephrocystins function at the TZ to dock and organize proteins destined for the cilium and that perturbing this universal process may have cell type–specific consequences on cilium structure and function.

Results

NPHP-1 and NPHP-4 are required for CEM cilia length and shape

NPHP-1 and NPHP-4 colocalize with the polycystins LOV-1 and PKD-2 in male-specific sensory neurons (Jauregui and Barr, 2005). Mutations in the polycystin-encoding genes cause autosomal dominant PKD (Igarashi and Somlo, 2002). To determine the function of the nephrocystins in polycystin-expressing neurons, we expressed NPHP-1::GFP and NPHP-4::GFP using

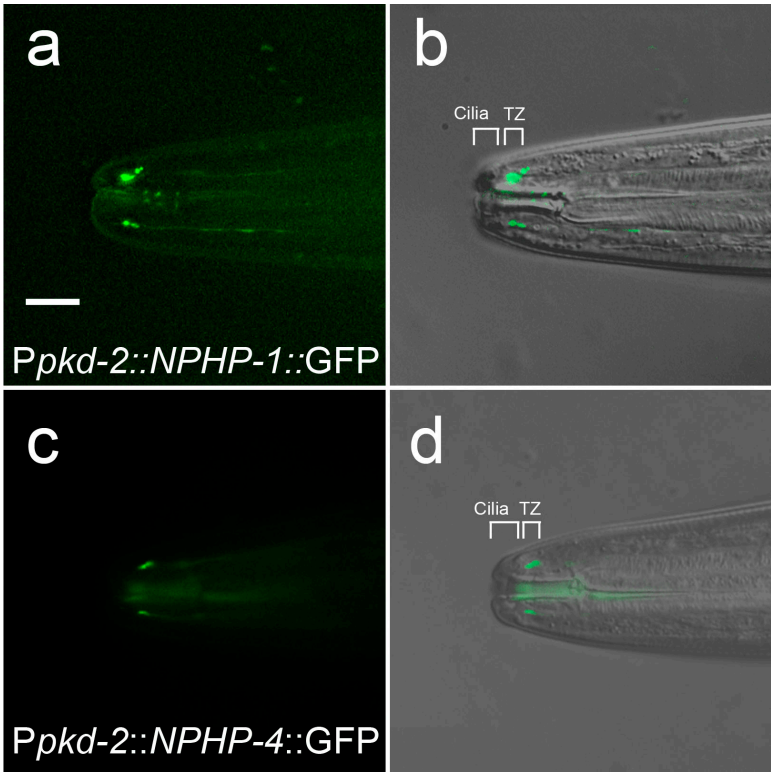

Figure 1. **NPHP-1 and NPHP-4 localize to TZs of male-specific CEM cilia.** 3D deconvolution images of NPHP-1::GFP (a) and NPHP-4::GFP (c) expressed only in male-specific CEM neurons and overlaid on Nomarski images (b and d). NPHP-1::GFP and NPHP-4::GFP localize to the CEM TZ but not the cilium proper (a–d). The CEM axoneme emanates from the TZ to the cuticle (territories of CEM cilium are indicated by brackets in b and d). Lateral view is shown. Bar, 10 μm.

the *pkd-2* promoter. NPHP-1 and NPHP-4 localize to the ciliary TZ in the CEM, RnB, and HOB male-specific neurons (Fig. 1) similar to nephrocystin TZ localization in amphid and phasmid neurons (Winkelbauer et al., 2005).

To examine ciliary architecture of male-specific neurons, we labeled CEM ciliary axonemes with β-tubulin TBB-4::GFP driven by the *pkd-2* promoter. Wild-type CEM cilia are ∼4.4 ± 0.6 μm in length and curve outward from the TZ (Figs. 2 c and S1 a; and Video 1, available at http://www.jcb.org/cgi/content/full/jcb.200707090/DC1). In *nphp-1* mutants, CEM cilia are stunted or misshaped (Figs. 2 f and S1 b; and Video 2). Stunted CEM cilia were posteriorly misplaced or did not reach the cuticle; misshapen CEM axonemes were morphologically variable, ranging from gentle curls forming fishhooks to extreme loops and inward bends. The stunted and misshapen cilia phenotypes have variable expressivity (Fig. 3 A). Misshapen/curly cilia were longer than the wild type (7.5 ± 1.8 vs. 4.4 ± 0.6 μm), whereas stunted cilia were shorter (3.3 ± 0.7 μm; Fig. 3 B).

nphp-4 CEM axonemes were also stunted or misshapen and long (Figs. 2 i, 3, and S1 c; and Video 3, available at http://www.jcb.org/cgi/content/full/jcb.200707090/DC1) but observed at a lower frequency compared with *nphp-1* mutants (15% vs. 45%). The *nphp-1;nphp-4* double mutant resembled the *nphp-4* single mutant (Fig. 3). These data indicate that *nphp-4* acts epistatically to *nphp-1* in CEM cilia and are consistent with the observation that NPHP-1 requires NPHP-4 to localize to the ciliary TZ (Winkelbauer et al., 2005). We conclude that the ciliary TZ proteins NPHP-1 and NPHP-4 regulate ciliary length and morphology in the polycystin-expressing CEM neurons.

nphp-4 mutants have ultrastructural defects in CEM, CEP, and OLQ cilia

We used transmission EM (TEM) to examine CEM ciliary ultrastructure of wild-type and *nphp-4* males, the latter of which was missing both NPHP-1 and NPHP-4 at the TZ. Wild-type CEM TZs are similar to the CEP and OLQ TZs (Perkins et al., 1986), with 9 + 0 microtubule doublets and Y-linked membrane attachments (Fig. 4 e). The CEM and CEP TZs are enclosed within the same sheath and socket cells. The wild-type CEM middle segment swells in diameter and displays many peripheral microtubule singlets and a few dispersed central microtubule singlets (Fig. 4, c and d). This is different from amphid channel cilia middle segments, which remain narrow and contain nine microtubule doublets comprised of A and B tubules (see Fig. 8 i). More anteriorly, the wild-type CEM axoneme winds around and away from the CEP cilium and OLQ distal region. CEM distal segments are narrow and contain many dark filled microtubule singlets (Fig. 4 b) reminiscent of distal segments of ray RnB cilia (Sulston et al., 1980). The most distal region of the CEM curves outward and is exposed to the environment via a narrow cuticular opening (Ward et al., 1975). Here, the CEM cilium typically bends by 90° to open laterally; thus, its microtubules are seen lengthwise in a transverse section (Fig. 4 a). CEP and OLQ distal segments end embedded in the cuticle at the nose tip (Perkins et al., 1986).

nphp-4 CEM cilia range from ultrastucturally normal to stunted or misshaped/long. Stunted CEM cilia lack distal microtubule singlets and do not extend to the cephalic cuticular opening (Fig. 4 f). In these stunted cilia, *nphp-4* CEM middle segments are typically enlarged (Fig. 4 h), whereas TZs appear normal

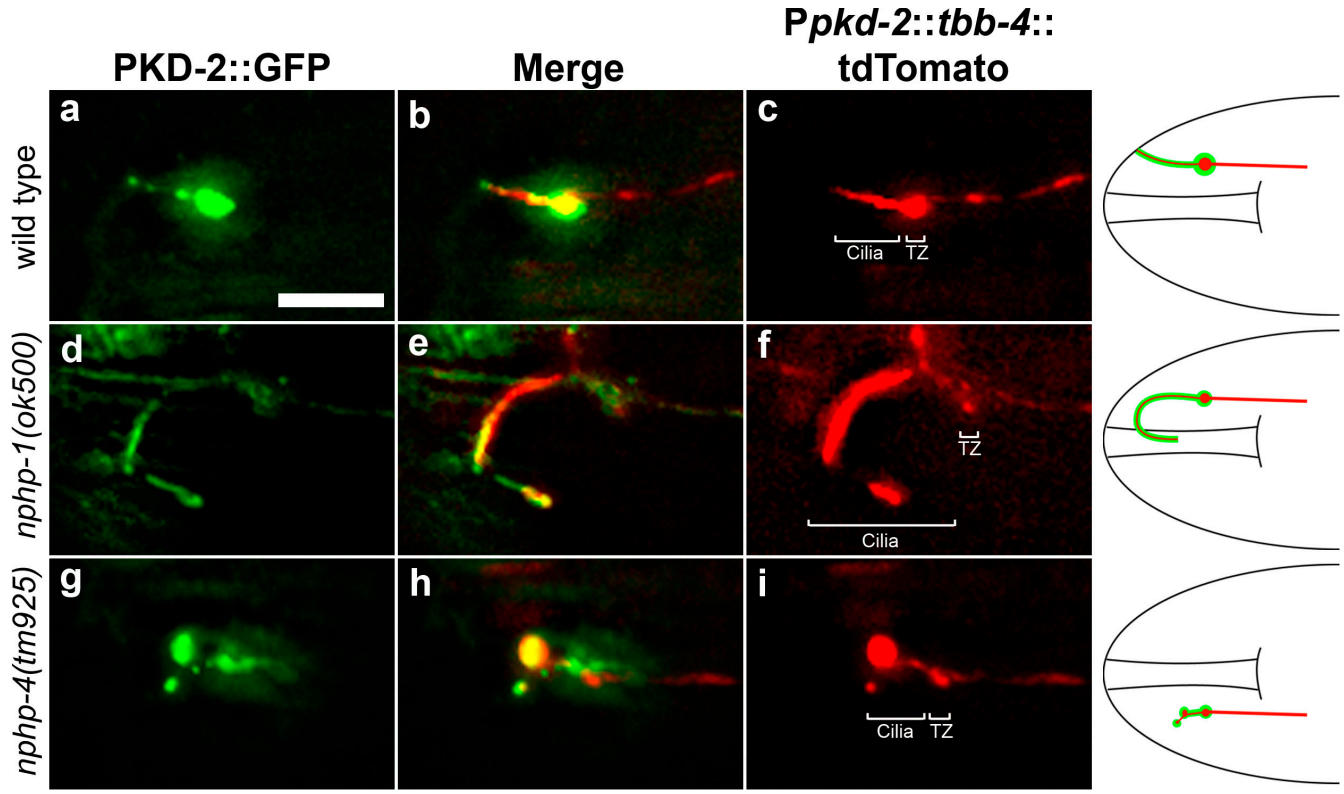

Figure 2. **PKD-2::GFP localizes to abnormally formed CEM cilia in *nphp-1* and *nphp-4* mutants.** 3D deconvolution images of a single CEM cilium in wild type (a–c), *nphp-1* (d–f), and *nphp-4* (g–i). See also Videos 1–3 (available at http://www.jcb.org/cgi/content/full/jcb.200707090/DC1). Cilium structure is labeled by β-tubulin (*Ppkd-2::tbb-4::tdTomato*; c, f, and i). PKD-2::GFP localizes to the TZ and cilium proper in the wild type (a), to abnormally curled *nphp-1* cilia (d), and to *nphp-4* stunted cilia (g). Drawings show relationship between reporters in context of the male nose. Bar, 5 μm.

(Fig. 4 i). Misshaped CEM cilia wander circuitously while traversing the sheath channel but middle segments appear fairly normal and distal segments usually reach the cuticular opening (unpublished data).

Ultrastructural defects are also seen in the nearby CEP and OLQ cilia of *nphp-4* animals. CEP cilia are enlarged and misshaped, and sometimes displaced posteriorly, elaborating their cilium within the sheath and socket without embedding in the cuticle (unpublished data). In wild-type CEP cilia, the majority of tubulin-associated material (TAM) is found in distal regions (Fig. 4, a and b). In *nphp-4* CEP cilia, large amounts of TAM are displaced into middle regions (Fig. 4 j), with dense aggregations and reduced amounts of TAM in distal segments (Fig. 4, g and h). *nphp-4* OLQ cilia are occasionally stunted (Fig. 4 f), distorted due to severed or missing microtubules (Fig. 4, g and h), or posteriorly misplaced (Fig. 4 i). In a few cases, the OLQ cilium may be truncated at or near the TZ. Although CEM and OLQ TZs appear normal, few CEP TZs were obtained in our slices, likely because of posterior displacement. We conclude that the TZ proteins NPHP-1 and NPHP-4 regulate ciliary length (OLQ and CEM), ciliary morphogenesis (CEM, CEP, and OLQ), and transport of axonemal components such as TAM (CEP).

NPHP-1 and NPHP-4 are not required for ciliary localization of TRP channels

NPHP-1 and/or NPHP-4 may regulate ciliary receptor localization. In wild-type CEMs, PKD-2::GFP accumulates at the TZ and localizes along the ciliary membrane (Qin et al., 2005; Bae et al., 2006), and the underlying ciliary axoneme follows this pattern (*Ppkd-2::tbb-4::tdTomato* in Fig. 2, a–c). In *nphp-1* mutants, PKD-2::GFP localizes and slightly accumulates around misshaped cilia (Fig. 2, d–f). In *nphp-4* mutants, PKD-2::GFP localizes to stunted cilia and accumulates at the TZ and distal dendrite (Fig. 2, g–i). We also examined the localization of the TRPV channel OSM-9, which localizes to OLQ, amphid, and phasmid cilia (Colbert et al., 1997; Tobin et al., 2002). In *nphp-1* and *nphp-4* mutants, OSM-9::GFP localizes to OLQ cilia that are occasionally misshaped or stunted (Fig. S2, available at http://www.jcb.org/cgi/content/full/jcb.200707090/DC1), which is consistent with TEM data (Fig. 4). We conclude that *nphp-1* and *nphp-4* are not essential for PKD-2 and OSM-9 ciliary localization.

nphp-4 regulates ciliary localization of a subset of IFT components

To determine the molecular basis for the stunted and deformed cilia, we examined the IFT machinery in *nphp-1* and *nphp-4* mutants. To measure IFT in CEM cilia, we used the *pkd-2* promoter to express the IFT-B polypeptide OSM-5 and observed OSM-5::GFP motility in wild-type CEM cilia, *nphp-4* stunted cilia, and *nphp-1* misshaped/long cilia (Videos 4–6, available at http://www.jcb.org/cgi/content/full/jcb.200707090/DC1). However, we were unable to measure IFT velocities because the CEMs curve out of the microscopic plane. As IFT has been

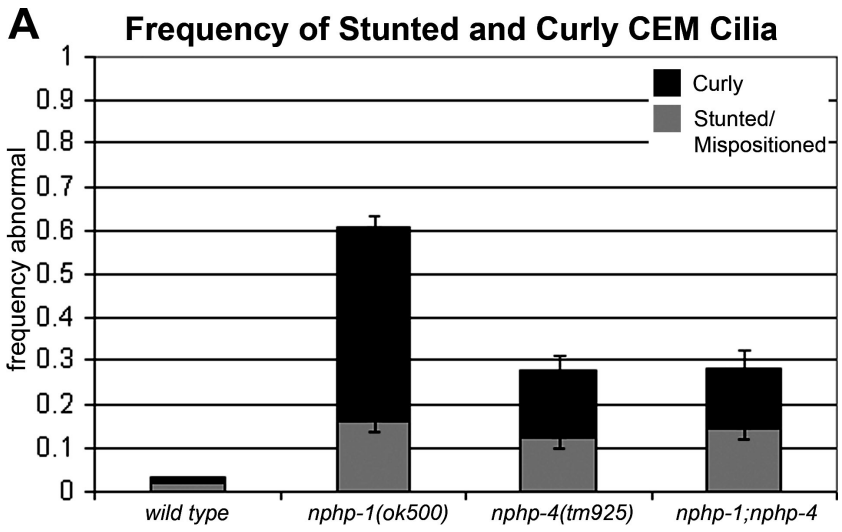

Figure 3. ***nphp-1* and *nphp-4* mutants have misshaped, long, and stunted cilia.** (A) CEM cilia are visualized using *Ppkd-2::tbb-4::GFP*. Dark gray indicates the frequency of misshaped curly CEM cilia; light gray indicates the frequency of stunted or mispositioned cilia. *nphp-1* mutants have predominantly curly CEM cilia with some stunted cilia. *nphp-4* and *nphp-1;nphp-4* mutants have equal numbers of stunted and curly cilia. At least 50 animals are scored per genotype (~200 individual CEM cilia are observed). Error bars indicate ±SEM. (B) CEM cilia were divided into wild-type, curly, and stunted categories. From z stack compressions of 3D wild-type and mutant CEM cilia; lengths were measured by tracing the cilium from the base of the TZ to the end of the axoneme. Curly cilia are significantly longer than the wild type. Stunted or misplaced cilia are slightly shorter than the wild type. The z distance of curls is not represented in this assay. p-values from a *t* test compare mutants to the wild type.

B

CEM Cilia Length Category

	Normal	Curly	P-val	Stunted	P-val
Wild type	4.4±0.6 (40)	-	-	-	-
nphp-1(ok500)	4.6±0.6 (48)	7.5±1.8 (56)	<0.001	3.3±0.7 (33)	<0.001
nphp-4(tm925)	4.7±0.5 (102)	8.2±1.6 (21)	<0.001	3.3±0.9 (36)	<0.001

extensively studied in amphid channel cilia (Scholey et al., 2004; Snow et al., 2004; Ou et al., 2005, 2007; Evans et al., 2006; Pan et al., 2006; Scholey and Anderson, 2006), we focused on these cilia types. We compared the localization patterns of GFP-tagged IFT motors, IFT-A and IFT-B polypeptides, and regulators in wild-type and nephrocystin-deficient cilia. In the *nphp-1* mutant, all IFT components localized similarly to the wild type (Fig. 5). Strikingly, in *nphp-4* single or *nphp-1;nphp-4* double mutants, some but not all IFT components exhibited abnormal ciliary localization patterns (Fig. 5, b3, b4, d4, e3, e4, f3, f4, i3, and i4).

In wild-type and *nphp-1* animals, IFT-A and IFT-B polypeptides localize to the ciliary TZs, middle segments, and distal segments (Fig. 5, a1, b1, c1, and d1). In *nphp-4* mutants, the complex B IFT52–OSM-6 polypeptide was noticeably dimmer in cilia, with weak a GFP signal in distal segments (Figs. 5 b3 and S3, available at http://www.jcb.org/cgi/content/full/jcb.200707090/DC1). In contrast, IFT-B polypeptides IFT88/Polaris/OSM-5 and IFT80/CHE-2 (not depicted) displayed normal localization patterns (Fig. 5 c). Occasionally, CHE-13::GFP was missing from distal segments of *nphp-4* and *nphp-1;nphp-4* animals (in 6 out of 23 animals; Fig. 5 d), although this has not been observed previously (Winkelbauer et al., 2005). IFT-A polypeptide CHE-11::GFP was normal in the single and double mutants (Fig. 5, a3 and a4).

We examined the IFT kinesin-2 motors and the BBS proteins, which are proposed to connect and stabilize kinesin-II and OSM-3. In the wild type, *nphp-1*, and *nphp-4* single and double mutants, kinesin-II (visualized by KAP-1::GFP) localizes only to the middle segment and is not detectable in the distal region (Fig. 5 j). In wild-type and *nphp-1* animals, OSM-3::GFP localizes to both the middle and distal segments (Fig. 5, i1 and i2). In a striking contrast, *nphp-4* and *nphp-1;nphp-4* mutants exhibited reduced ciliary levels and increased dendritic levels of OSM-3::GFP (Fig. 5, i3 and i4). In wild-type and *nphp-1* animals, BBS-7::GFP and BBS-8::GFP localize to the TZ and along the middle and distal segments of the cilium (Fig. 5, e1, e2, f1, and f2). In *nphp-4* and *nphp-1;nphp-4* distal segments, BBS-7::GFP was dim or occasionally absent in distal segments (Fig. 5, e3 and e4), although this reduction was not as severe as observed for OSM-6::GFP. BBS-7::GFP occasionally aggregated between the middle and distal segments (Fig. 5 e3, arrow). Unlike BBS-7, BBS-8 did not appear to aggregate at the middle–distal segment boundary. However, BBS-8::GFP was extremely dim in middle and distal segments (Fig. 5, f3 and f4). Seven BBS proteins form a stable biochemical complex (the "BBSome"; Nachury et al., 2007). Our data suggests that in the absence of NPHP-1 and NPHP-4 at the TZ, the stoichiometry of the BBSome in the cilium may be altered.

We analyzed regulators of kinesin-2 activity. Dye filling defective (DYF)-1 has been proposed to activate OSM-3 (Ou et al., 2005) or regulate tubulin posttranslational modifications (Pathak et al., 2007). DYF-1::GFP did not have an overt mislocalization defect in *nphp-1* or *nphp-4* single or double mutants (Fig. 5 g), which suggests that OSM-3 dendritic accumulation in *nphp-4* mutants is DYF-1 independent. The *dyf-13* mutant, similar to *nphp-4* animals, occasionally lacks OSM-6::GFP in amphid distal segments (Blacque et al., 2005; Ou et al., 2005). DYF-13::GFP localization is intact in *nphp-1* and *nphp-4* single and double mutants (Fig. 5, h1–h4).

In conclusion, loss of both NPHP-1 and NPHP-4 but not NPHP-1 alone leads to the abnormal ciliary localization of the IFT-B polypeptide OSM-6, the OSM-3-kinesin, and the BBS proteins BBS-7 and BBS-8. In contrast, NPHP-1 and NPHP-4 are not required for the localization of the IFT-B polypeptides OSM-5 and CHE-2, IFT-A polypeptide CHE-11, kinesin-II, and ciliogenic proteins DYF-1 and DYF-13.

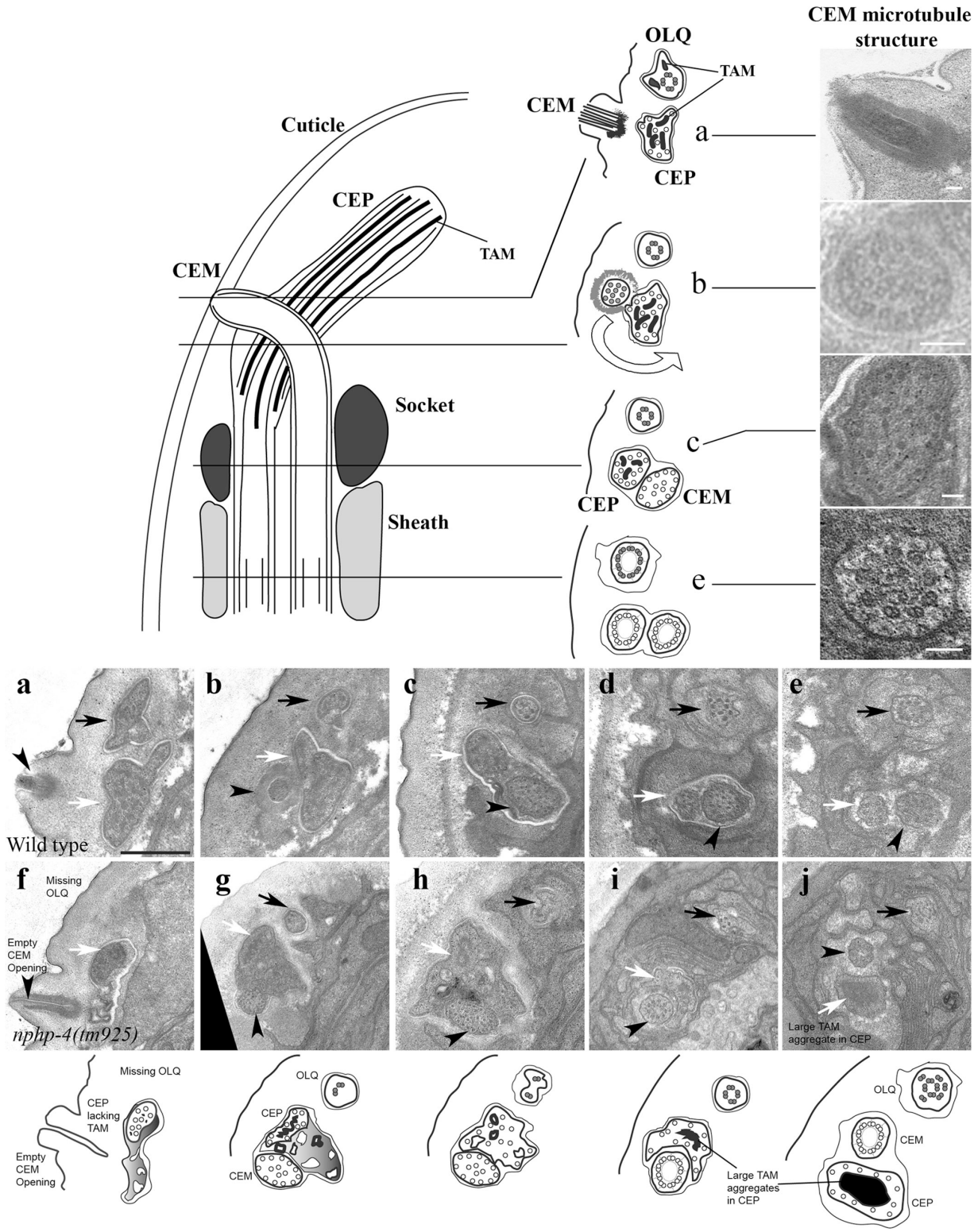

Figure 4. **CEM, CEP and OLQ ciliary ultrastructure is abnormal in *nphp-4* mutants.** TEM of wild type (a–e) and *nphp-4* (f–j) mutant animals in transverse thin sections. Black arrows, OLQ; white arrows, CEP; arrowheads, CEM. As depicted in the top drawings, the distal-most region of the CEM axoneme is narrow, curved outward, and exposed to the environment. Microtubule singlets are seen longitudinally near the opening (a). Traveling posteriorly, the distal segment aligns with the body axis and nears the edge of CEP socket cell (b). The CEM middle segment widens and is filled with microtubule outer singlets and dispersed inner singlets (c). The middle segment twists around the CEP away from the OLQ such that the CEM axoneme is furthest away from OLQ (d). CEM TZs are similar to CEP and OLQ TZs with 9 + 0 microtubule doublets (e). In *nphp-4* mutants, OLQ distal segments are occasionally missing (f) but middle segments are present (g) with missing microtubules (g and h). CEM and OLQ TZs appear normal (i and j). CEP axonemes are irregular with large unidentified accumulations (g–i). Panel j is from a different section of the same worm illustrating well-formed OLQ and CEM TZs but apparently missing a CEP TZ, replaced by a large mass of TAM surrounded by microtubule singlets. CEM axonemes can lack distal segments (empty channel in f with no microtubules). Drawings at bottom illustrate *nphp-4* defects. Bars: (top) 100 nm; (bottom) 0.5 μm.

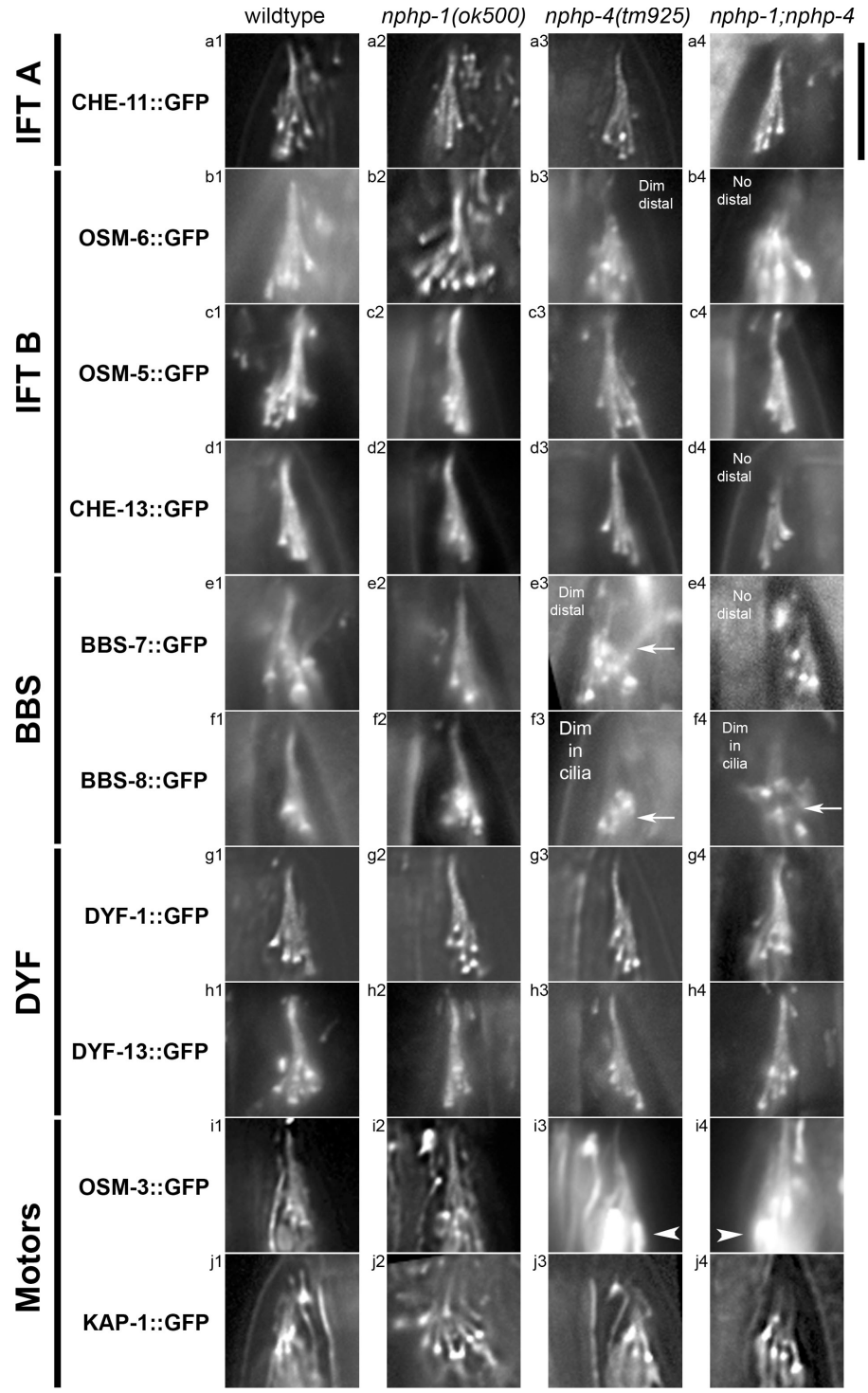

Figure 5. **The localization of some IFT components is affected in *nphp-4* mutants.** Amphid channel cilia expressing various IFT reporters in wild-type and nephrocystin mutants. In nephrocystin mutants, CHE-11::GFP (a1–a4), CHE-2::GFP (not depicted), and OSM-5::GFP (c1–c4) appear normal. In contrast, complex B polypeptide OSM-6::GFP is dimmer in amphid cilia and fails to enter or is restricted from the distal segment of *nphp-4* and *nphp-1;nphp-4* (b1–b4). In b3, "Dim distal" segments are observed and in b4, distal segments are not visible, indicated by "No distal." See Fig. S3 (available at http://www.jcb.org/cgi/content/full/jcb.200707090/DC1) for qualitative analysis of dim cilia. CHE-13::GFP (d1-d4) is normal in *nphp-1* mutants (d2) but is absent from the distal segment in 26% of *nphp-4* animals (d3 and d4). d3 is an example of amphid channel cilia that appeared normal, and d4 depicts amphid channel cilia lacking distal expression of CHE-13::GFP. BBS-7::GFP is also restricted from *nphp-4* and *nphp-1;nphp-4* distal segments (e3 and e4) and slightly aggregates in middle segments (e3, arrow). In *nphp-4*, BBS-8::GFP (f1–f4) was dim and barely detectable and "dim in cilia," although clearly present in TZs (f3 and f4, arrows). Localization of both DYF-1::GFP (g1–g3) and DYF-13::GFP (g1–g4) appears normal. OSM-3::GFP is considerably dimmer in *nphp-4* and *nphp-1;nphp-4* amphid cilia with bright signal in the distal dendrite (i3 and i4, arrowheads). KAP-1::GFP localization also appears normal, with no distal localization (j1–j4). Similar results were observed in phasmid cilia (not depicted). Lateral view of the lips is shown, the anterior is to the top of each panel. Bar, 10 μm.

nphp-4 mutation perturbs the velocity distributions of most IFT components examined

We measured IFT rates of kinesin-II, OSM-3, representative IFT-A (CHE-11) and IFT-B polypeptides (OSM-5 and OSM-6), BBS-7, and DYF-1 (Table I). KAP-1 velocities were indistinguishable between the wild type and *nphp* mutants. OSM-3, OSM-5, CHE-11, BBS-7, and DYF-1 are not significantly different between wild-type and nephrocystin-deficient animals. However, their underlying population of velocities in the middle segment of *nphp-4* and *nphp-1;nphp-4* animals was significantly different from the wild type (Table I, f-test), indicating that these IFT components are traveling at a wider range of speeds. Noncanonical IFT velocities have been observed by genetic mutations in vivo or by varying concentrations of kinesin-II and OSM-3 in vitro (Pan et al., 2006; Mukhopadhyay et al., 2007). We propose that by genetically perturbing the composition of the IFT machinery, abnormal velocities may emerge.

Table I. **Transport velocities of GFP tagged IFT proteins in wild-type and nephrocystin mutant animals**

Reporters	Genotype	Middle segment				Distal segment	
		Mean velocity (μm/s)	*n*	*t* test	f-test	Mean velocity (μm/s)	*n*
Kinesin-2 motors							
KAP-1::GFP	Wild type	0.69 ± 0.09	446			None	
	nphp-1	0.69 ± 0.09	420	0.49	0.4	None	
	nphp-4	0.68 ± 0.09	375	0.66	0.93	None	
	nphp-1;nphp-4	0.68 ± 0.09	423	0.77	0.46	None	
OSM-3::GFP	Wild type	0.72 ± 0.07	128			1.22 ± 0.14	145
	nphp-1	0.72 ± 0.07	81	0.9	0.37	1.18 ± 0.15	76
	nphp-4	0.83 ± 0.15	101	<0.001	<0.001	1.16 ± 0.14	55
	nphp-1;nphp-4	0.81 ± 0.15	213	<0.001	<0.001	1.03 ± 0.14	124
IFT particle A							
CHE-11::GFP	Wild type	0.71 ± 0.09	119			1.13 ± 0.15	119
	nphp-1	0.72 ± 0.08	131	0.9	0.22	1.19 ± 0.15	95
	nphp-4	0.74 ± 0.14	252	0.09	<0.001	1.11 ± 0.16	144
	nphp-1;nphp-4	0.74 ± 0.13	350	0.04	<0.001	1.06 ± 0.18	125
IFT particle B							
OSM-6::GFP	Wild type	0.71 ± 0.08	219			1.14 ± 0.16	218
	nphp-1	0.70 ± 0.09	98	0.48	0.25	1.26 ± 0.14	98
	nphp-4	0.49 ± 0.06	132	<0.001	0.02	1.07 ± 0.17	104
	nphp-1;nphp-4	0.47 ± 0.07	57	<0.001	0.2	ND	-
	nphp-4;kap-1	None	-	-	-	None	-
	kap-1 bbs-7;nphp-4	None	-	-	-	None	-
	osm-3	0.50 ± 0.07	252	<0.001	0.22	None	-
	osm-3;nphp-4	0.51 ± 0.06	221	<0.001	0.006	None	-
OSM-5::GFP	Wild type	0.71 ± 0.06	125			1.06 ± 0.16	132
	nphp-1	0.72 ± 0.08	281	0.567	0.004	1.07 ± 0.12	163
	nphp-4	0.75 ± 0.13	336	<0.001	<0.001	1.03 ± 0.14	132
	nphp-1;nphp-4	0.76 ± 0.15	472	<0.001	<0.001	1.05 ± 0.13	233
DYF proteins							
DYF-1::GFP	Wild type	0.72 ± 0.08	194			1.18 ± 0.14	139
	nphp-1	0.70 ± 0.09	83	0.17	0.15	1.07 ± 0.16	84
	nphp-4	0.77 ± 0.16	107	<0.001	<0.001	1.06 ± 0.16	80
	nphp-1;nphp-4	0.76 ± 0.16	167	<0.001	<0.001	1.04 ± 0.16	130
BBS proteins							
BBS-7::GFP	Wild type	0.68 ± 0.08	23			1.14 ± 0.16	56
	nphp-1	0.70 ± 0.07	110	0.19	0.63	1.15 ± 0.16	148
	nphp-4	0.82 ± 0.19	100	<0.001	<0.001	1.01 ± 0.23	56
	nphp-1;nphp-4	0.78 ± 0.17	66	<0.001	<0.001	1.02 ± 0.14	31

IFT velocities in wild type and nephrocystin mutants. The velocities of many IFT components are altered in *nphp-4* and *nphp-1;nphp-4* but not *nphp-1* animals. Distal segment velocities were similar to the wild type except for the slow OSM-6::GFP rates. Mean difference was shown statistically by a *t* test, whereas statistical variance difference was shown by an analysis of variance test f-test.

Unexpectedly, OSM-6::GFP velocity was dramatically affected by *nphp-4* mutation, slowing to 0.49 μm/s in the middle segment of *nphp-4* and *nphp-1;nphp-4* animals (Table I) and suggesting that overexpressed OSM-6::GFP is now traveling with endogenous kinesin-II alone. In dim distal segments of *nphp-4* mutants, OSM-6::GFP moved at 1.1 μm/s, the normal and predicted velocity of the fast kinesin OSM-3 (Table I). To test the hypothesis that OSM-6::GFP was abnormally associated with endogenous kinesin-II in the absence of *nphp-4*, we examined OSM-6::GFP in a *kap-1;nphp-4* double mutant. In these animals, OSM-6::GFP severely aggregates at ciliary bases and distal dendrites of amphid and phasmid sensory neurons (Fig. 6, j and n), and no IFT is detected. Conversely, in an *osm-3*;*nphp-4* double mutant, OSM-6::GFP was detected in the middle segments (Fig. 6, k and o) and moved at 0.5 μm/s (Table I). These results are consistent with OSM-6::GFP association with endogenous kinesin-II in *nphp-4* mutant cilia.

To determine if OSM-6::GFP was capable of associating with endogenous OSM-3, we examined OSM-6::GFP distribution in a *kap-1 bbs-7;nphp-4* triple mutant (Fig. 6, l and p). In *kap-1;bbs-7* double mutants, kinesin-II cargo is shifted to OSM-3 (Pan et al., 2006). *kap-1 bbs-7;nphp-4* phenotypically resembles the *kap-1;nphp-4* double mutant. OSM-6::GFP remains aggregated at the ciliary base and distal dendrite (Fig. 6, l and p), which indicates that OSM-6::GFP is incapable of associating with the endogenous IFT-B subcomplex–OSM-3 motor unit in the absence of *nphp-4*.

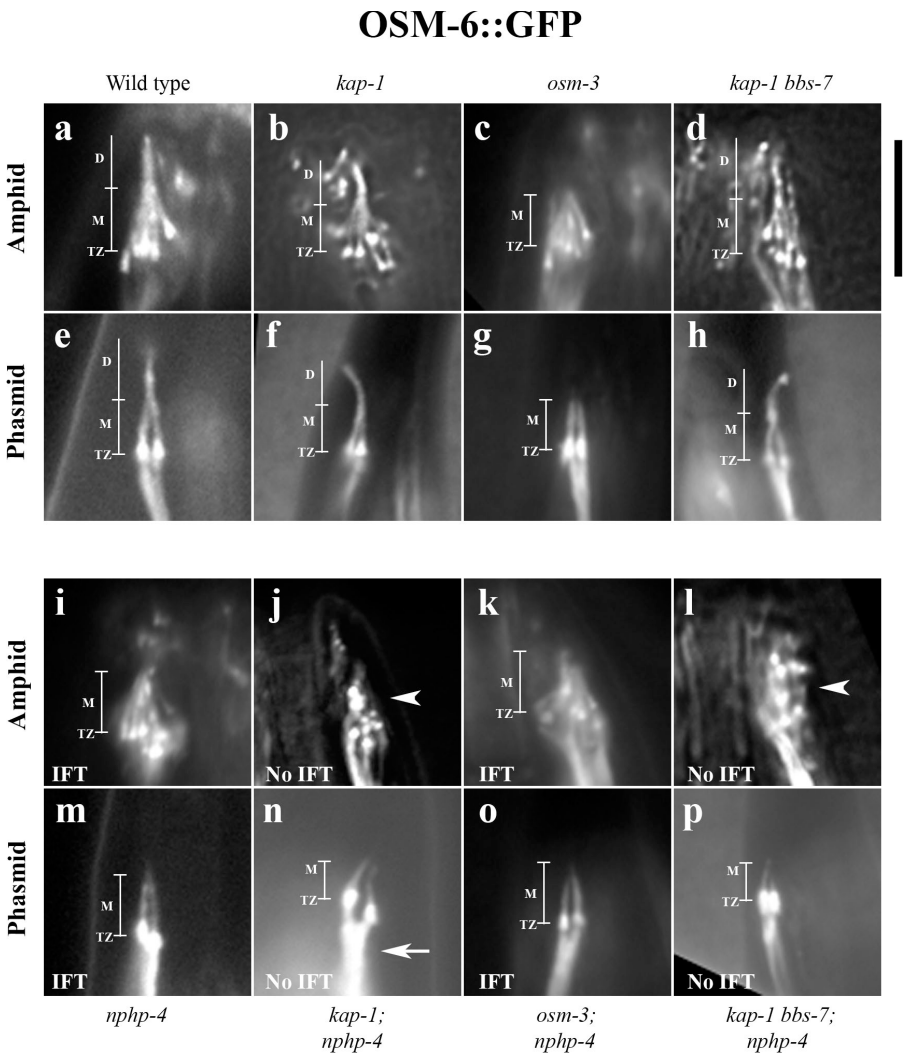

Figure 6. **IFT-B polypeptide OSM-6::GFP abnormally associates with kinesin-II in *nphp-4* mutants.** OSM-6::GFP in amphid (a–d and i–l) and phasmid (e–h and m–p) cilia in various IFT and *nphp-4* mutants. The IFT-B polypeptide OSM-6::GFP enters ciliary distal segments in *kap-1* and *kap-1;bbs-7* single and double mutants (b and f and d and h). OSM-6::GFP localizes to middle segments of *osm-3* mutants (c and g) and is absent from missing distal segments. In *kap-1;nphp-4* and *kap-1;bbs-7;nphp-4* animals, OSM-6::GFP severely aggregates in amphid cilia (j and l, arrowhead) and fails to enter distal segments (j and n and l and p). The arrow in panel n indicates dendritic accumulation of OSM-6::GFP. No IFT is detected, though slight amounts of OSM-6::GFP passively enter severely stunted cilia (n and p). In contrast, IFT is detected in *nphp-4;osm-3* double mutants (k and o; Table I). Brackets indicate separation of middle (M), distal (D), and TZ regions of cilia. (a–d) Lateral view of the lips; the anterior is to the top. (e–h) Lateral view of the tail; posterior is to the top. Bar, 10 μm.

Overexpression of certain elements of the IFT machinery is toxic to nephrocystin-deficient cilia

Lipophilic fluorescent dye filling of amphid and phasmid neurons is routinely used to diagnose defects in cilium structure (Hedgecock et al., 1985; Inglis et al., 2006). IFT-A, IFT-B, and *osm-3* mutants are all Dyf (Fig. 7 c; Perkins et al., 1986). In contrast, kinesin-II mutants are non-Dyf (Fig. 7 b) and have subtle effects on cilium formation and function but obviously affect ciliary transport at the molecular level (Snow et al., 2004; Ou et al., 2005; Bae et al., 2006; Evans et al., 2006; Mukhopadhyay et al., 2007). Likewise, *nphp-1* and *nphp-4* single and double mutants have no obvious dye filling defects (Jauregui and Barr, 2005; Winkelbauer et al., 2005) but subtly affect cilia formation at the ultrastructural and molecular levels (this paper). It was puzzling that *nphp-4* mutants perturbed the IFT machinery and yet had no overt dye filling defects. We therefore reexamined dye filling in *nphp-4* mutants using a more sensitive assay with reduced DiI concentration and shorter incubation time and observed partial Dyf defects (Fig. 7, d and f).

Because OSM-6::GFP exhibited abnormal motility rates in middle segments and was largely absent from distal segment of *nphp-4* mutants, we examined ciliary integrity of these strains via DiI labeling. In the absence of the OSM-6::GFP array, *nphp-4* single and *nphp-4;kap-1* double mutants were weakly Dyf (Fig. 7, d and e). To our surprise, the OSM-6::GFP array produced a strong Dyf phenotype in combination with the *nphp-4* mutation (Fig. 7, j–l). In the *nphp-4* background, we also observed more severe Dyf defects with BBS-7::GFP and very weak enhancement of Dyf defects with BBS-8::GFP and OSM-3::GFP. In contrast, properly localized IFT components (OSM-5::GFP and KAP-1::GFP) do not affect ciliogenesis in the *nphp-4* background (unpublished data). This synthetic Dyf (SynDyf) defect was only observed in *nphp-4* mutants, as OSM-6::GFP, BBS-7::GFP, BBS-8::GFP, and OSM-3::GFP are not reported to enhance ciliogenic defects in other genetic backgrounds (Collet et al., 1998; Snow et al., 2004; Ou et al., 2005, 2007). We propose that the nephrocystins functionally interact with OSM-6 and select IFT components at the TZ. When NPHP-1 and NPHP-4 are missing from the TZ, overexpression of certain elements of the IFT machinery is toxic to cilia (Fig. S4, available at http://www.jcb.org/cgi/content/full/jcb.200707090/DC1).

nphp-4 mutants have B tubule defects in amphid channel cilia

To correlate molecular and biophysical defects in IFT at the ultrastructural level, we used TEM to examine *nphp-4* amphid

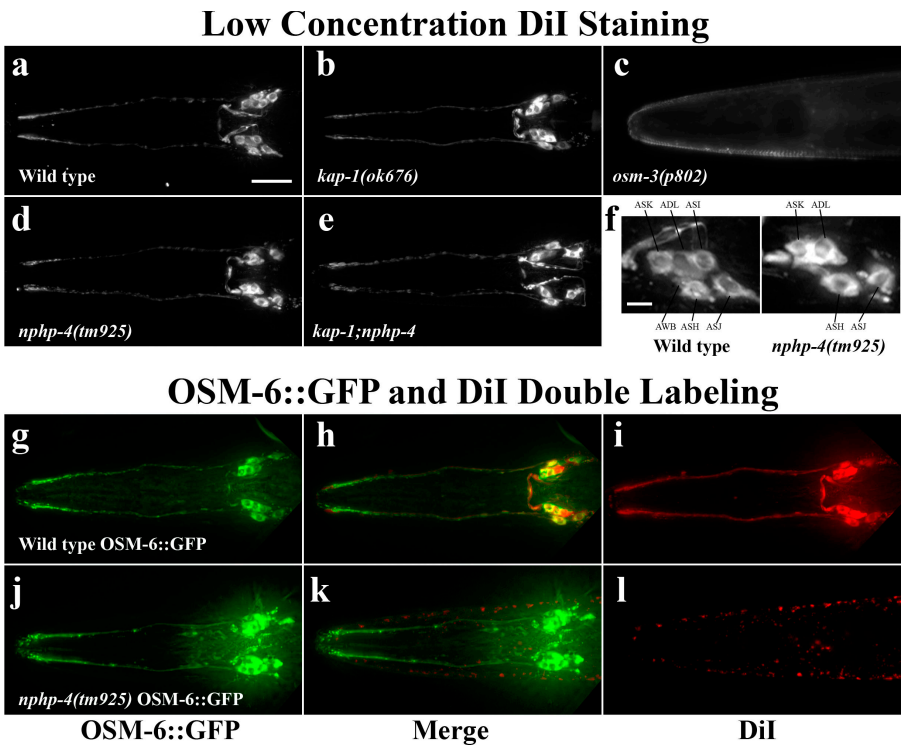

Figure 7. **OSM-6::GFP overexpression in *nphp-4* mutants results in a severe SynDyf phenotype.** Compression of a 3D deconvoluted z stack of amphid ciliated neurons filled with DiI. Wild type (a) and *kap-1* mutants (b) fill with DiI. In contrast, *osm-3* animals (c) lacking distal segments of cilia fail to fill with DiI. Some but not all amphid neurons fill with DiI in *nphp-4* single (d) and *kap-1;nphp-4* double mutants (e). Panel f is a 2.5× view of wild-type and *nphp-4* neuron cell bodies that filled with dye. There is slight variability in the neurons that fail to fill between individual animals. The OSM-6::GFP transgene in the *nphp-4* mutant background causes a SynDyf defect (j–l). The *mnIs17* OSM-6::GFP transgene does not interfere with dye filling in the wild type (g–i) or *kap-1* or *nphp-1* mutants (not depicted), nor does OSM-6::GFP interfere with ciliogenesis in any published reports (Collet et al., 1998; Snow et al., 2004; Ou et al., 2005). Bars: (a) 20 μm; (f) 5 μm.

channel cilia (Fig. 8). Wild-type and *nphp-4* TZs appeared similar, with the characteristic 9 + 0 microtubule doublet pattern drawn together by an apical ring and attached to the membrane by Y links (Fig. 8, c and f). Wild-type amphid channel middle and distal segments consist of nine doublet (A tubule and B tubule; Fig. 8 j) and nine singlet (A tubule only) microtubules, respectively. In *nphp-4* middle segments, one or two doublet microtubules were occasionally missing entirely or deformed and more often prematurely reduced to singlets (Fig. 8 e). Some middle segments possessed abnormal microtubule singlets lacking the B tubule (Fig. 8, e and i, arrowhead), abnormal doublets with a truncated B tubule, or open B tubules (Fig. 8 i, arrows). In both wild-type and *nphp-4* animals, ADL amphid cilia typically showed inner seam openings of all or most B tubules along most of the middle segment (Fig. 8, g–i). Openings at an outer seam of the B tubule were very rare, as were lateral openings of the B tubule (unpublished data). In the wild type, most surrounding amphid cilia showed few or no open B tubules, except for ASI, where more limited inner seam breaks occurred with regularity over short portions.

In *nphp-4* mutant amphid channel cilia, B tubule inner seam breaks were increased in number and in linear dimension (compare Fig. 8, k–m, to the wild type in Fig. 8 j). In *nphp-4* animals, ADL cilia still showed the highest degree of inner seam breaks (Fig. 8, g and m), and ASI seam breaks were more common and extended over much of the middle segment (Fig. 8 k). ASI is one of the two neurons that does not fill with DiI in *nphp-4* animals (Fig. 7 f). In *nphp-4* mutants, smaller, limited inner seam breaks also occurred in ASJ (Fig. 8, g and l) and to a lesser extent in ASG, ASH, and ASK cilia (Fig. 8 i). In affected cilia other than ADL and ASI, individual microtubules generally showed small seam breaks at random along the middle segment, with two to five microtubules interrupted per ciliary axoneme, often not at the same level. Occasionally, one middle segment was missing entirely, with 9 rather than 10 cilia in the amphid channel (Fig. 8 e). Because true serial thin sections along the entire amphid channel were not collected, we cannot always determine which cilia are truncated, but some truncations involved cilia with unusual B tubule seam breaks in nearby portions of the middle segment (including ASJ and ASH). Two to four amphid distal segments were often missing, likely because of premature truncation of the distal segments of some cilia (Fig. 8 d). Intact distal segments contained normal microtubule singlets. We conclude that *nphp-4* mutations do not disrupt TZ formation but do result in axonemal defects in a cell type–specific manner.

Discussion

NPHP is one of several human diseases that share the features of ciliary localized gene products and cystic kidneys (for review see Hildebrandt and Zhou, 2007). *C. elegans* nephrocystin-1 and nephrocystin-4 homologues have been implicated in signal transduction (Jauregui and Barr, 2005; Winkelbauer et al., 2005; Wolf et al., 2005). Here, we rule out a role for the nephrocystins in ciliary receptor localization of TRPP channel PKD-2 and the TRPV channel OSM-9 (Figs. 2 and S2). Instead, we demonstrate for the first time that nephrocystin-1 and nephrocystin-4 act globally at the TZ to modulate ciliary development and morphogenesis in a cell type–specific manner. The human nephrocystins also localize to the TZ of renal and respiratory epithelial cells and photoreceptors (Mollet et al., 2005; Otto et al., 2003, 2005; Fliegauf et al., 2006), which suggests an evolutionarily conserved function.

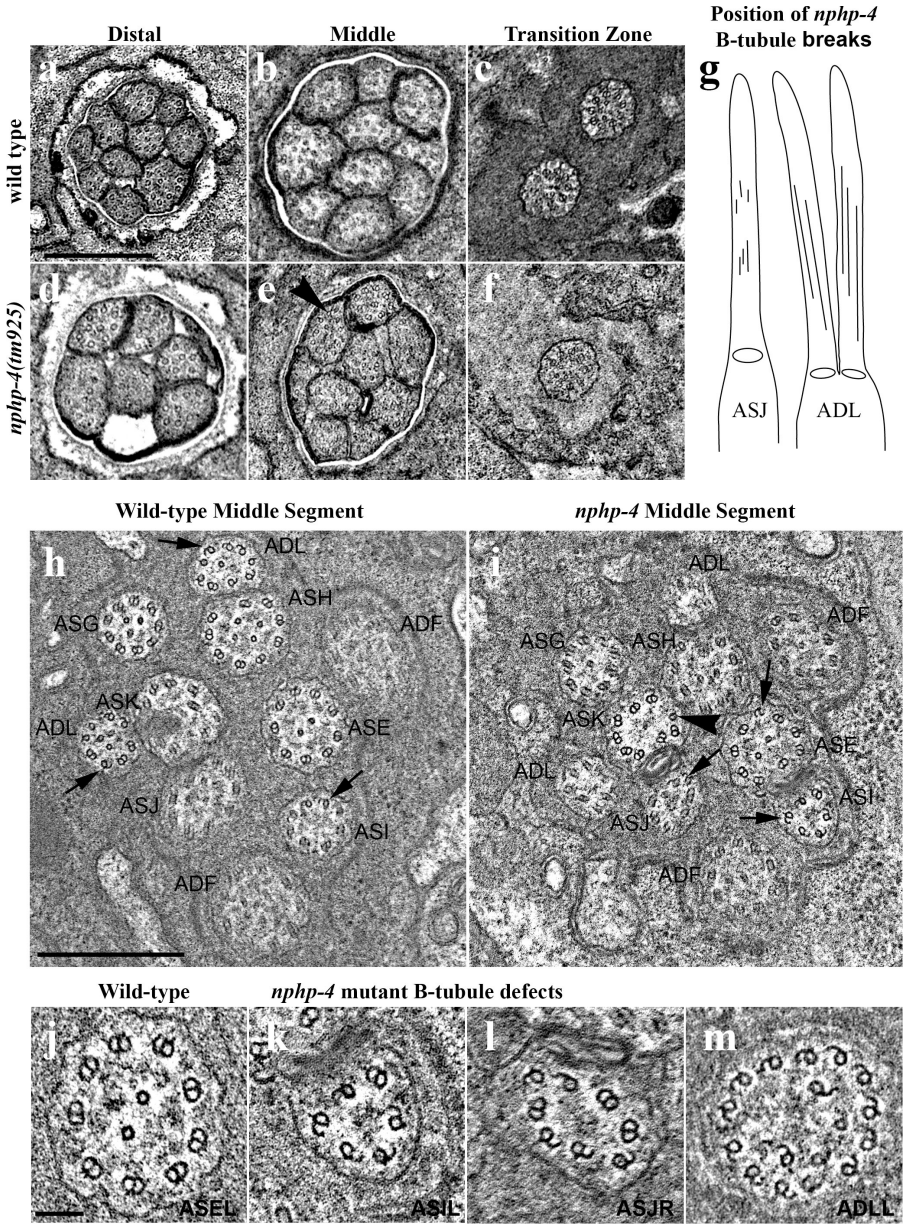

Figure 8. **Amphid cilia are shortened and have abnormal microtubule structure in *nphp-4* mutants.** TEM of amphid channel cilia in the wild type (a–c, h, and j) and *nphp-4* (d–f, i, and k–m). In *nphp-4*, some distal segments are shortened; panel d shows 6 out of the normal 10 distal segments that should be present. Middle segments (e, i, and m) are sometimes swollen or withered. Because of slight cilia bending, views of individual microtubules within a cilium are sometimes seen obliquely and seem distorted; when tilted in the microscope, those distortions go away. Occasionally the channel contains <10 cilia; in panel e, nine are present, suggesting that at least one cilium is completely absent past the TZ. Some middle segments have microtubule doublets abnormally converting prematurely to singlets lacking B tubules (e and i, arrowhead) or abnormal doublets with an inner seam break of the B tubule (i, arrows), whereas others appear normal. Such inner seam breaks are also found in wild-type cilia of ADL and ASI (h, arrows) but become much more common in other cilia in *nphp-4* (i, k, and l). Schematic cartoon (g) displays the region of the middle segment where seam breaks are common in ADL (wild type and mutant) and in ASJ mutant cilia, seen from a lateral aspect. In wild-type and *nphp-4* ADL cilia, all microtubules tend to have long continuous seam breaks. In ASJ, shorter, discontinuous seam breaks are scattered along the middle segment, but only in *nphp-4* animals. Small spurs can also be seen on the outer surface of many A tubules within the middle segment, looking vaguely similar to Y-link features of the axoneme (compare c with k–m). Panel m shows a *nphp-4* ADL cilium, just distal to the axoneme, where an increased number of microtubule doublets surround the outer edge (13 rather than 8–9), most showing B tubule seam breaks; some inner "singlets" even have partial B tubules. This represents a fused cilium (seen in 2/6 amphids in *nphp-4*); ADL normally forms two separate cilia (g). (i) An electron-dense mass that may represent jammed IFT particles. TZs are typically well-formed in *nphp-4* mutants (f). Bars: (a) 0.5 μm; (h) 0.5 μm; (j) 100 nm.

The *C. elegans* nephrocystins act broadly to regulate cilium structure in a cell type–specific capacity

Previous experiments using DiI as an indicator of cilium structure suggested that *nphp-1* and *nphp-4* were not required for ciliogenesis (Jauregui and Barr, 2005; Winkelbauer et al., 2005). However, these dyes only fill amphid and phasmid cilia. A more rigorous diagnosis using fluorescently labeled ciliary components combined with TEM ultrastructural analysis revealed a broad range of ultrastructural defects in many cilia types. For example, the CEMs of nephrocystin mutants may be excessively long and curled, which suggests that the nephrocystins regulate ciliary morphogenesis and length. In the mechanosensory CEPs, TAM is mislocalized in *nphp-4* mutant cilia, which suggests a role for the transport of axonemal components. In amphid channel distal regions, *nphp-4* mutants contain six to eight of the normal complement of 10 cilia, indicating that NPHP-1 and NPHP-4 contribute to ciliary development. In *nphp-4* middle segments, microtubule axonemal defects include missing or incomplete B tubules, which suggests that the nephrocystins may be required for A–B microtubule stability (Stephens, 2000). Interestingly, similar B tubules defects have been observed in the hennin/arl13b GTPase mutant mouse, which has defects in ciliary development and sonic hedgehog signaling (Caspary et al., 2007).

Although *nphp-4* ciliary ultrastructural defects vary depending on cell type, two generalities may be drawn. First, there is variable phenotypic expressivity within a type of cilium. However, the frequency of *nphp-4* CEM ciliary defects (~30%; Fig. 3) is similar to the frequency of *nphp-4* amphid channel defects (4 of 10 distal segments are missing; Fig. 8). Variable phenotypic expressivity is also observed in NPHP patients. Second, *nphp-4* ultrastructural defects appear not in the TZ but occur principally in the middle segment, raising the question of how the NPHP-1

and NPHP-4 TZ proteins act. Rosenbaum and Witman (2002) have proposed that the transition fibers at the base of the *C. reinhardtii* flagellum serve as a "flagellar pore complex" to restrict the access of proteins to the cilium. At the bioinformatics level, some IFT proteins are related by sequence to components of the nuclear pore complex (Jekely and Arendt, 2006). At the ultrastructural level, transition fibers form physical links between basal body microtubules and the flagellar membrane (Ringo, 1967; Weiss et al., 1977). At the molecular level, most of the IFT particles accumulate at the basal body (Cole et al., 1998; Pazour et al., 1999). The *C. elegans* ciliary TZ also possesses links from microtubules to the membrane and accumulates IFT motors and polypeptides (Figs. 4 e and 8 f; Perkins et al., 1986). Unlike IFT components that localize to the TZ and ciliary compartment, the *C. elegans* nephrocystins localize to the TZ and are not detected in the cilium proper (Fig. 1; Jauregui and Barr, 2005; Winkelbauer et al., 2005). Notably, immunoelectron microscopy shows that IFT52 (homologous to *C. elegans* OSM-6) associates at the periphery of transition fibers, leading to the proposal that this region serves as an IFT docking site (Deane et al., 2001). Our data suggests that NPHP-4 and OSM-6 functionally interact to regulate ciliogenesis (Figs. 7 and S4).

In amphid channel neurons, *nphp-4* mutations (lacking both NPHP-1 and NPHP-4 at the TZ) increased B tubule breaks in the middle segment, which in turn likely affected IFT velocity distributions (Table I, f-test column). We propose that NPHP-1 and NPHP-4 may indirectly regulate the balance between the IFT motors, control the composition of individual IFT particles with a cilium, and/or modulate IFT in a cell type–specific manner that is masked by an average taken from 10 axonemes. In this respect, it is notable that a minority of cilia within the amphid bundle exhibit different assembly patterns even in the wild type, including a pronounced weakness at the inner seam junction between A and B tubules. These structural weaknesses become more general in the *nphp-4* mutant cilia, now affecting the majority of all cilia.

Surprisingly, IFT-B polypeptide OSM-6::GFP moved at the slow kinesin-II rate in *nphp-4* and *nphp-1;nphp-4* middle segments and produced the SynDyf phenotype, reflecting a severe defect in ciliogenesis. The former result is not predicted by the current IFT model, whereby the kinesin-II/IFT-A and OSM-3/IFT-B units are linked by the BBS proteins (Ou et al., 2005, 2007). However, IFT-A may travel with OSM-3 and IFT-B may travel with kinesin-II in a *bbs;kinesin-2* double mutant, indicating that genetic background influences IFT complex constituents in vivo (Pan et al., 2006). The latter results indicate that OSM-6::GFP overexpression is toxic to *nphp-4* cilia. Why OSM-6 is an outlier is not resolved. However, OSM-6 is different from other IFT polypeptides with respect to the *C. elegans* mutant phenotype (Perkins et al., 1986; Collet et al. 1998) and domain structure (Beatson and Ponting, 2004; Jekely and Arendt 2006). Although mutations in the IFT-B polypeptide encoding genes *osm-1*, *osm-5*, and *che-13* disrupt middle and distal amphid segments, the *osm-6* mutant has a less severe phenotype, primarily lacking distal segments (Perkins et al., 1986). With the exception of OSM-6/IFT52 and the GTPase IFT27, IFT polypeptides contain WD40, TRP, or coiled-coil protein–protein interaction domains (Jekely and Arendt 2006). OSM-6 contains a GIFT domain, for which a sugar-binding role is proposed (Beatson and Ponting, 2004), and a proline-rich region, which is predicted to bind SH3 domains (Collet et al., 1998). Interestingly, NPHP-1 contains an SH3 domain (Jauregui and Barr 2005; Wolf et al., 2005). Given that mammalian nephrocystin-1 and nephrocystin-4 physically associate (Mollet et al., 2002), it is tempting to speculate that they form a ternary complex with OSM-6/IFT52 at the TZ.

Cilia length control and the nephrocystins

The misshaped and long CEM cilia of *nphp-1* and *nphp-4* mutants are unique. The nature of this defect is not known, nor do we know the reason for the higher frequency of misshaped cilia in *nphp-1* animals. Marshall et al. (2005) have proposed that ciliary length is controlled by a balance between ciliary assembly and disassembly and that disrupting this balance could result in long, short, or no cilia (Wemmer and Marshall, 2007). Human nephrocystin interacts with nephrocystin-2/inversin, a protein that binds to β-tubulin (Otto et al., 2003; Nurnberger et al., 2004), and nephrocystin-3, a protein that contains a tubulin tyrosine ligase (TTL) domain (Olbrich et al., 2003). TTLs and other tubulin modification enzymes catalyze tubulin posttranslational modifications, which regulate axonemal microtubules and perhaps IFT (Janke et al., 2005; Redeker et al., 2005; Pathak et al., 2007; Stephan et al., 2007). In *C. elegans*, the ODR-3 G α protein, kinesin-II, and the mitogen-activated protein kinase DYF-5 regulate ciliary morphogenesis and length in a cell type–specific manner (Roayaie et al., 1998; Bae et al., 2006; Evans et al., 2006; Burghoorn et al., 2007). In mammalian cells, overexpression or constitutive activation of the Rab8 GDP/GTP exhange factor results in abnormally long cilia (Nachury et al., 2007; Yoshimura et al., 2007). In $Bbs4^{-/-}$ mice, primary cilia length is also increased (Mokrzan et al., 2007). The NIMA (never in mitosis A) kinase *nek8* is mutated in human *NPHP9* patients and the juvenile cystic kidney (*jck*) mouse model, which has primary cilia that are significantly longer than in the wild type (Smith et al., 2006; Otto et al., 2008). Mislocalization or misregulation of these types of proteins may cause defects in ciliary length or shape in nephrocystin mutants (Fig. S4).

Genetic modifiers in cilia development, maintenance, and function

Loss of the nephrocystins may sensitize cells to ciliogenic defects, explaining why overexpression of some IFT components in the absence of *nphp-4* increases ciliary defects (Fig. 7, j–l; and Fig. S4). Genetic and functional redundancy is a mechanism to ensure normal development and protect against disease. Intriguingly, genetic modifier loci may account for extrarenal symptoms associated with NPHP (Parisi et al., 2004; Tory et al., 2007), and oligogenicity is observed in some NPHP patients (Hoefele et al., 2007). In the *pcy*/NPHP3 mouse, genetic background affects the cystic phenotype (Guay-Woodford, 2003). In humans, NPHP has clinical phenotypes that overlap Joubert and Meckel syndromes (Delous et al., 2007).

Biochemical approaches have been used to study the physical interactions of IFT components (Cole et al., 1998; Cole,

2003; Qin et al., 2004; Lucker et al., 2005). Genetic approaches may be exploited to identify functional relationships between ciliary proteins. In the budding yeast, functional interactions are determined by a synthetic dosage lethality phenotype, where overexpression of a normally nontoxic gene induces lethality in the context of a viable mutant (Kroll et al., 1996). For example, a genome-wide synthetic dosage lethal screen identified 141 nonessential deletion mutants that cannot tolerate overexpression of kinetochore genes (Measday et al., 2005). We propose that SynDyf screens, in which overexpression of predicted cilioproteins (such as OSM-6::GFP) in non-Dyf or partial Dyf ciliary mutants (such as *nphp-4*) exacerbates the Dyf defect, will reveal functional rather than physical interactions. This type of strategy will allow for the systematic dissection of proteins involved in ciliogenesis and potentially identify genetic modifier loci and candidates for human disease genes. Genetic analysis in simple animal models will continue to progress our understanding of human ciliopathies.

Materials and methods

C. elegans mutant alleles and strains

Nematodes were raised using standard conditions (Brenner, 1974). The following mutant alleles were used. LGII: *nphp-1(ok500)*; LGIII: *pha-1(e2123)* and *kap-1(ok676)*; LGIV: *pkd-2(sy606)* and *myIs1[PKD-2::GFP]*; and LGV: *him-5(e1490)*, *nphp-4(tm925)*, *bbs-7(ok1351)*, and *mnIs17[OSM-6::GFP;unc36(+)]*. The *him-5(e1490)* allele was crossed into all strains to increase the frequency of males and represents the wild type in all assays. Some strains were obtained from the Caenorhabditis Genetics Center and the Japanese Bioresource Project for the Nematode C. elegans. The *mnIs17* OSM-6::GFP reporter strain was provided by R. Herman and J. Collet (University of Minnesota, Minneapolis, MN) and some IFT fluorescent reporter strains were provided by J. Scholey and G. Ou (University of California, Davis, Davis, CA).

The following general strains were used. CB1490: *him-5(e1490)*; PT9: *pkd-2(ok606);him-5(e1490)*; PT1036: *nphp-1(ok500);him-5(e1490)*; PT1038: *nphp-4(tm925),him-5(e1490)*; and PT1040: *nphp-1(ok500); nphp-4(tm925),him-5(e1490)*.

The following transgenic strains were used. PT1283: *pha-1(e2123); him-5(e1490);myEx516[Ppkd-2::nphp-1::GFP;pBX]*; PT1247: *pha-1(e2123); him-5(e1490);myEx514[Ppkd-2::nphp-4::GFP;pBX]*; PT1435: *pha-1(e2123); him-5(e1490);myIs1[PKD-2::GFP]; myEx552[Ppkd-2::tbb-4::tdTomato;pBX]*; PT1437: *nphp-1(ok500); pha-1(e2123); him-5(e1490); myIs1[PKD-2::GFP]; myEx552[Ppkd-2::tbb-4::tdTomato;pBX]*; PT1439: *pha-1(e2123);nphp-4(tm925)* and *him-5(e1490);myIs1[PKD-2::GFP];myEx552[Ppkd-2::tbb-4::tdTomato;pBX]*; PT1017: *pha-1(e2123); him-5(e1490); myEx470[Ppkd-2::tbb-4::GFP;pBx]*; PT980: *nphp-1(ok500); pha-1(e2123);him-5(e1490); myEx470[Ppkd-2::tbb-4::GFP;pBx]*; PT982: *pha-1(e2123);nphp-4(tm925), him-5(e1490);myEx470[Ppkd-2::tbb-4::GFP; pBx]*; PT984: *nphp-1(ok500); pha-1(e2123); nphp-4(tm925)* and *him-5(e1490);myEx470[Ppkd-2::tbb-4::GFP;pBx]*; PT443: *pkd-2(sy606);myIs1[PKD-2::GFP];him-5(e1490)*; PT667: *nphp-1(ok500);pkd-2(sy606);myIs1[PKD-2::GFP];him-5(e1490)*; PT834: *pkd-2(sy606);nphp-4(tm925);myIs1 [PKD-2::GFP];him-5(e1490)*; and PT836: *nphp-1(ok500);pkd-2(sy606); nphp-4(tm925);myIs1[PKD-2::GFP];him-5(e1490)*.

The following IFT reporter strains were used. PT50: *Ex[CHE-11::GFP + pRF4]*; PT1332: *nphp-1(ok500);Ex[CHE-11::GFP]*; PT1333: *nphp-4(tm925);Ex[CHE-11::GFP]*; PT1335: *nphp-1(ok500);nphp-4(tm925); Ex[CHE-11::GFP]*; SP2101: *mnIs17[OSM-6::GFP]*; PT1119: *nphp-1(ok500); mnIs17[OSM-6::GFP;unc-36(+)]*; PT1121: *nphp-4(tm925);mnIs17[OSM-6::GFP;unc-36(+)]*; PT1123: *nphp-1(ok500);nphp-4(tm925);mnIs17[OSM-6::GFP;unc-36(+)]*; PT1349: *nphp-1(ok500);Ex[BBS-7::GFP]*; PT1351: *nphp-4(tm925);Ex[BBS-7::GFP]*; PT1353: *nphp-1(ok500);nphp-4(tm925); Ex[BBS-7::GFP]*; PT1336: *nphp-1(ok500);Ex[DYF-1::GFP]*; PT1337: *nphp-4(tm925);Ex[DYF-1::GFP]*; PT1339: *nphp-1(ok500);nphp-4(tm925);Ex[DYF-1::GFP]*; PT1341: *nphp-1(ok500);Ex[OSM-3::GFP]*; PT1343: *nphp-4(tm925); Ex[OSM-3::GFP]*; PT1344: *nphp-1(ok500);nphp-4(tm925);Ex[OSM-3::GFP]*; PT1346: *nphp-1(ok500);Ex[KAP-1::GFP]*; PT1347: *nphp-4(tm925);Ex[KAP-1::GFP]*; PT1348: *nphp-1(ok500);nphp-4(tm925);Ex[KAP-1::GFP]*; PT1402: *nphp-1(ok500);Ex[CHE-2::GFP]*; PT1404: *nphp-4(tm925);Ex[CHE-2::GFP]*; PT1406: *nphp-1(ok500);nphp-4(tm925);Ex[CHE-2::GFP]*; PT1408: *nphp-1(ok500);Ex[OSM-5::GFP]*; PT1410: *nphp-4(tm925);Ex[OSM-5::GFP]*; PT1412: *nphp-1(ok500);nphp-4(tm925);Ex[OSM-5::GFP]*; PT1417: *nphp-1(ok500);Ex[CHE-13::GFP]*; PT1420: *nphp-4(tm925);Ex[CHE-13::GFP]*; PT1421: *nphp-1(ok500);nphp-4(tm925);Ex[CHE-13::GFP]*; PT1429: *nphp-1(ok500);Ex[BBS-8::GFP]*; PT1431: *nphp-4(tm925);Ex[BBS-8::GFP]*; PT1433: *nphp-1(ok500);nphp-4(tm925);Ex[BBS-8::GFP]*; PT1423: *nphp-1(ok500);Ex[DYF-13::GFP]*; PT1425: *nphp-4(tm925);Ex[DYF-13::GFP]*; PT1427: *nphp-1(ok500)nphp-4(tm925);Ex[DYF-13::GFP]*; PT1524: *kap-1(ok676);nphp-4(tm925);him-5(e1490);mnIs17[OSM-6::GFP]*; PT1609: *kap-1(ok676);bbs-7(ok1351);mnIs17[OSM-6::GFP]*; PT1524: *kap-1(ok676); nphp-4(tm925);him-5(e1490);mnIs17[OSM-6::GFP]*; PT1610: *kap-1(ok676);bbs-7(ok1351);nphp-4(tm925);mnIs17[OSM-6::GFP]*; PT1653: *osm-3(p802);mnIs17[OSM-6::GFP]*; and PT1655: *osm-3(p802);nphp-4(tm925);him-5(e1490);mnIs17[OSM-6::GFP]*.

Fluorescent reporters

GFP or tandem dimer Tomato (tdTomato; obtained from R. Tsien, University of California, San Diego, La Jolla, CA) was used as a reporter for all expression constructs. *Ppkd-2::NPHP-1::GFP* (pAJ6) and *Ppkd-2::NPHP-4::GFP* (pAJ7) was generated by PCR addition of SphI and KpnI restriction sites to *nphp-1* and *nphp-4* cDNAs followed by cloning into pPD95.75 containing the 1.3-kb *pkd-2* promoter (pKK5). *Ppkd-2::tbb-4::GFP* has been described previously (Bae et al., 2006). To generate *Ppkd-2::tbb-4::tdTomato*, tdTomato was PCR modified to add AgeI and EcoRI restriction sites such that tdTomato replaces the GFP insert of *Ppkd-2::tbb-4::GFP* to create *Ppkd-2::tbb-4::tdTomato* (pAJ8).

Dye-filling assay

Standard dye-filling assays were performed (Perkins et al., 1986). Alternatively, reduced dye concentration and incubation time were used. A 2 mg/ml DiD or DiI (Invitrogen) in dimethyl formamide stock was diluted 1:1,000 in M9. Worms were incubated for <30 min in this solution and washed three times with M9.

Microscopy

Animals were raised at 20°C and imaged at 25°C using standard *C. elegans* slide mounts and Plan Apochroma 63× 1.4 oil differential interference contrast (DIC), 100× 1.3 oil DIC, or 100× 1.4 oil DIC objectives (Carl Zeiss, Inc.) on an imaging microscope (Axioplan 2; Carl Zeiss, Inc.). Fluorochromes used were either eGFP or tdTomato. CEM cilia were visualized using *Ppkd-2::tbb-4::GFP* that labels cell bodies, dendrites/axons, and cilia. Frequency of abnormally stunted or curly CEM cilia was scored for at least 50 animals scored per genotype. Wild-type animals have four CEM cilia that gently curve outward toward the cuticle. Stunted was defined as shortened or misplaced CEM axonemes that did not traverse the distance to the cuticle and lacked gentle outward curvature. Curly CEM cilia were defined as axonemes that were typically longer than the wild type and had strong curvature. Those CEM cilia that were difficult to image were not categorized. The score for each animal was determined by the number of abnormal CEM cilia divided by the total number of scorable CEM cilia. Percentages were then averaged to determine a population mean. To measure CEM cilia length, a z stack was taken and compressed into a single image. The CEM cilia were then traced using Metamorph software (MDS Analytical Technologies) and the length was recorded and averaged.

IFT motility was observed with an Axioplan 2 imaging microscope using a Plan APOCHROMA 100× 1.3 or 1.4 NA oil objective (Carl Zeiss, Inc.). Motility stacks were recorded using a camera (Photometrics Cascade 512B; Roper Scientific), and kymographs and the particle movement rate were measured using Metamorph software. Strains were synchronized by picking L4 worms, culturing at 15°C overnight, and imaging within 24 h. Worms were anesthetized in a drop of M9 containing 10 mM muscimol, transferred to an agarose mount slide, and imaged immediately.

"Dim in cilia" is defined as significantly reduced fluorescence of IFT::GFP reporters in cilia compared with the wild type (Fig. S3). For mutants with "dim cilia," threshold adjustments were increased to visualize cilia. Additionally, "dim distal" is defined as amphid distal segments that have significantly reduced fluorescence of IFT::GFP reporters when compared with adjacent middle segments. The basis of the "dim" phenotype is likely a combination of reduced number of distal segments in the amphid channel and reduced frequency of IFT particles entering the distal segment.

For TEM, worms were fixed in 3% glutaraldehyde in cacodylate buffer on ice. Then, heads were cut off, moved to fresh fixative, and held in fix

overnight at 4°C. Animals were rinsed in buffer and stained with 1% osmium tetroxide in cacodylate buffer for 1 hr at 4°C. After embedding in small groups in agarose, the specimens were en bloc stained with 1% uranyl acetate in sodium acetate buffer, dehydrated, and embedded in Embed812 resin according to the general procedures described by Hall (1995). Thin sections were collected on a diamond knife and post-stained before being viewed on a CM10 electron microscope (Philips; Hall, 1995). Details in wild-type amphid cilia microtubule architecture were reconfirmed in additional adult animals fixed by high-pressure freezing followed by freeze substitution (Rostaing et al., 2004). This analysis (not depicted) reconfirmed the strong tendency of ADL and ASI cilia to suffer inner seam breaks of the B tubule, eliminating any chance that the microtubule defects were a fixation artifact.

Software for image processing with operations involved AutoDeblur 1.4.1 (Media Cybernetics, Inc.), which was used only for 3D blind deconvolution, and Photoshop (Adobe), which was used for image rotation, cropping, brightness/contrast, and filter "unsharp mask" for TEM and for generation of all figures.

Online supplemental material

Fig. S1 shows that CEM cilia are curled or stunted in nephrocystin mutant *C. elegans*. Fig. S2 shows that OLQ cilia are misshapen in nephrocystin mutants. Fig. S3 shows that OSM-6::GFP is dim in *nphp-4* amphid and phasmid cilia. Fig. S4 shows a model for NPHP-1 and NPHP-4 function. Videos 1–3 show a 3D reconstruction of wild-type and nephrocystin mutant CEM cilia. Videos 4–6 show IFT of P*pkd-2*::OSM-5::GFP in wild-type and nephrocystin CEM cilia. Online supplemental material is available at http://www.jcb.org/cgi/content/full/jcb.200707090/DC1.

We thank the *Caenorhabditis* Genetics Center, the Japanese Bioresource Project, R. Herman, G. Ou, and J. Scholey for strains; R. Tsien for the tdTomato construct; Y.K. Bae for time-lapse microscopy assistance; D. Braun for technical excellence; and J. Jauregui and J. Wolfe for invaluable support during the laboratory relocation. We also appreciate new insights provided by our reviewers.

This work was funded by the PKD Foundation (grant 74b2r to M.M. Barr) and the National Institutes of Health (grants 1F31DK076202, 5R24RR012596, and 5R01DK074746 to A.R. Jauregui, D.H. Hall, and M.M. Barr, respectively).

Submitted: 12 July 2007
Accepted: 7 February 2008

References

Arts, H.H., D. Doherty, S.E. van Beersum, M.A. Parisi, S.J. Letteboer, N.T. Gorden, T.A. Peters, T. Marker, K. Voesenek, A. Kartono, et al. 2007. Mutations in the gene encoding the basal body protein RPGRIP1L, a nephrocystin-4 interactor, cause Joubert syndrome. *Nat. Genet.* 39:882–888.

Attanasio, M., N.H. Uhlenhaut, V.H. Sousa, J.F. O'Toole, E. Otto, K. Anlag, C. Klugmann, A.C. Treier, J. Helou, J.A. Sayer, et al. 2007. Loss of GLIS2 causes nephronophthisis in humans and mice by increased apoptosis and fibrosis. *Nat. Genet.* 39:1018–1024.

Badano, J.L., N. Mitsuma, P.L. Beales, and N. Katsanis. 2006. The ciliopathies: an emerging class of human genetic disorders. *Annu. Rev. Genomics Hum. Genet.* 7:125–148.

Bae, Y.K., H. Qin, K.M. Knobel, J. Hu, J.L. Rosenbaum, and M.M. Barr. 2006. General and cell-type specific mechanisms target TRPP2/PKD-2 to cilia. *Development.* 133:3859–3870.

Bargmann, C.I. 2006. Related comparative chemosensation from receptors to ecology. *Nature.* 444:295–301.

Barr, M.M. 2005. *Caenorhabditis elegans* as a model to study renal development and disease: sexy cilia. *J. Am. Soc. Nephrol.* 16:305–312.

Barr, M.M., and P.W. Sternberg. 1999. A polycystic kidney-disease gene homologue required for male mating behaviour in *C. elegans*. *Nature.* 401:386–389.

Barr, M.M., J. DeModena, D. Braun, C.Q. Nguyen, D.H. Hall, and P.W. Sternberg. 2001. The *Caenorhabditis elegans* autosomal dominant polycystic kidney disease gene homologs *lov-1* and *pkd-2* act in the same pathway. *Curr. Biol.* 11:1341–1346.

Beales, P.L., E. Bland, J.L. Tobin, C. Bacchelli, B. Tuysuz, J. Hill, S. Rix, C.G. Pearson, M. Kai, J. Hartley, et al. 2007. IFT80, which encodes a conserved intraflagellar transport protein, is mutated in Jeune asphyxiating thoracic dystrophy. *Nat. Genet.* 39:727–729.

Beatson, S., and C.P. Ponting. 2004. GIFT domains: linking eukaryotic intraflagellar transport and glycosylation to bacterial gliding. *Trends Biochem. Sci.* 29:396–399.

Blacque, O.E., M.J. Reardon, C. Li, J. McCarthy, M.R. Mahjoub, S.J. Ansley, J.L. Badano, A.K. Mah, P.L. Beales, W.S. Davidson, et al. 2004. Loss of *C. elegans* BBS-7 and BBS-8 protein function results in cilia defects and compromised intraflagellar transport. *Genes Dev.* 18:1630–1642.

Blacque, O.E., E.A. Perens, K.A. Boroevich, P.N. Inglis, C. Li, A. Warner, J. Khattra, R.A. Holt, G. Ou, A.K. Mah, et al. 2005. Functional genomics of the cilium, a sensory organelle. *Curr. Biol.* 15:935–941.

Brenner, S. 1974. The genetics of *Caenorhabditis elegans*. *Genetics.* 77:71–94.

Burghoorn, J., M.P. Dekkers, S. Rademakers, T. de Jong, R. Willemsen, and G. Jansen. 2007. Mutation of the MAP kinase DYF-5 affects docking and undocking of kinesin-2 motors and reduces their speed in the cilia of *Caenorhabditis elegans*. *Proc. Natl. Acad. Sci. USA.* 104:7157–7162.

Caridi, G., M. Dagnino, A. Rossi, E.M. Valente, E. Bertini, E. Fazzi, F. Emma, L. Murer, E. Verrina, and G.M. Ghiggeri. 2006. Nephronophthisis type 1 deletion syndrome with neurological symptoms: prevalence and significance of the association. *Kidney Int.* 70:1342–1347.

Caspary, T., C.E. Larkins, and K.V. Anderson. 2007. The graded response to Sonic Hedgehog depends on cilia architecture. *Dev. Cell.* 12:767–778.

Colbert, H.A., T.L. Smith, and C.I. Bargmann. 1997. OSM-9, a novel protein with structural similarity to channels, is required for olfaction, mechanosensation, and olfactory adaptation in *Caenorhabditis elegans*. *J. Neurosci.* 17:8259–8269.

Cole, D.G. 2003. The intraflagellar transport machinery of *Chlamydomonas reinhardtii*. *Traffic.* 4:435–442.

Cole, D.G., S.W. Chinn, K.P. Wedaman, K. Hall, T. Vuong, and J.M. Scholey. 1993. Novel heterotrimeric kinesin-related protein purified from sea urchin eggs. *Nature.* 366:268–270.

Cole, D.G., D.R. Diener, A.L. Himelblau, P.L. Beech, J.C. Fuster, and J.L. Rosenbaum. 1998. *Chlamydomonas* kinesin-II–dependent intraflagellar transport (IFT): IFT particles contain proteins required for ciliary assembly in *Caenorhabditis elegans* sensory neurons. *J. Cell Biol.* 141:993–1008.

Collet, J., C.A. Spike, E.A. Lundquist, J.E. Shaw, and R.K. Herman. 1998. Analysis of *osm-6*, a gene that affects sensory cilium structure and sensory neuron function in *Caenorhabditis elegans*. *Genetics.* 148:187–200.

Deane, J.A., D.G. Cole, E.S. Seeley, D.R. Diener, and J.L. Rosenbaum. 2001. Localization of intraflagellar transport protein IFT52 identifies basal body transitional fibers as the docking site for IFT particles. *Curr. Biol.* 11:1586–1590.

Delous, M., L. Baala, R. Salomon, C. Laclef, J. Vierkotten, K. Tory, C. Golzio, T. Lacoste, L. Besse, C. Ozilou, et al. 2007. The ciliary gene RPGRIP1L is mutated in cerebello-oculo-renal syndrome (Joubert syndrome type B) and Meckel syndrome. *Nat. Genet.* 39:875–881.

Evans, J.E., J.J. Snow, A.L. Gunnarson, G. Ou, H. Stahlberg, K.L. McDonald, and J.M. Scholey. 2006. Functional modulation of IFT kinesins extends the sensory repertoire of ciliated neurons in *Caenorhabditis elegans*. *J. Cell Biol.* 172:663–669.

Fliegauf, M., J. Horvath, C. von Schnakenburg, H. Olbrich, D. Muller, J. Thumfart, B. Schermer, G.J. Pazour, H.P. Neumann, H. Zentgraf, et al. 2006. Nephrocystin specifically localizes to the transition zone of renal and respiratory cilia and photoreceptor connecting cilia. *J. Am. Soc. Nephrol.* 17:2424–2433.

Guay-Woodford, L.M. 2003. Murine models of polycystic kidney disease: molecular and therapeutic insights. *Am. J. Physiol. Renal Physiol.* 285:F1034–F1049.

Hall, D.H. 1995. Electron microscopy and three-dimensional image reconstruction. *Methods Cell Biol.* 48:395–436.

Hall, D.H., and R.L. Russell. 1991. The posterior nervous system of the nematode *Caenorhabditis elegans*: serial reconstruction of identified neurons and complete pattern of synaptic interactions. *J. Neurosci.* 11:1–22.

Hedgecock, E.M., J.G. Culotti, J.N. Thomson, and L.A. Perkins. 1985. Axonal guidance mutants of *Caenorhabditis elegans* identified by filling sensory neurons with fluorescein dyes. *Dev. Biol.* 111:158–170.

Hildebrandt, F., and W. Zhou. 2007. Nephronophthisis-associated ciliopathies. *J. Am. Soc. Nephrol.* 18:1855–1871.

Hildebrandt, F., E. Otto, C. Rensing, H.G. Nothwang, M. Vollmer, J. Adolphs, H. Hanusch, and M. Brandis. 1997. A novel gene encoding an SH3 domain protein is mutated in nephronophthisis type 1. *Nat. Genet.* 17:149–153.

Hoefele, J., M.T. Wolf, J.F. O'Toole, E.A. Otto, U. Schultheiss, G. Deschenes, M. Attanasio, B. Utsch, C. Antignac, and F. Hildebrandt. 2007. Evidence of oligogenic inheritance in nephronophthisis. *J. Am. Soc. Nephrol.* 18:2789–2795.

Igarashi, P., and S. Somlo. 2002. Genetics and pathogenesis of polycystic kidney disease. *J. Am. Soc. Nephrol.* 13:2384–2398.

Inglis P.N., G. Ou, M.R. Leroux, and J.M. Scholey. 2006. The sensory cilia of *Caenorhabditis elegans*. *Wormbook*, editor. The *C. elegans* Research

Community, WormBook, doi/10.1895/wormbook.1.126.1, http://www.wormbook.org (accessed March 8, 2007).

Janke, C., K. Rogowski, D. Wloga, C. Regnard, A.V. Kajava, J.M. Strub, N. Temurak, J. van Dijk, D. Boucher, A. van Dorsselaer, et al. 2005. Tubulin polyglutamylase enzymes are members of the TTL domain protein family. *Science.* 308:1758–1762.

Jauregui, A.R., and M.M. Barr. 2005. Functional characterization of the *C. elegans* nephrocystins NPHP-1 and NPHP-4 and their role in cilia and male sensory behaviors. *Exp. Cell Res.* 305:333–342.

Jekely, G., and D. Arendt. 2006. Evolution of intraflagellar transport from coated vesicles and autogenous origin of the eukaryotic cilium. *Bioessays.* 28:191–198.

Keller, L.C., E.P. Romijn, I. Zamora, J.R. Yates III, and W.F. Marshall. 2005. Proteomic analysis of isolated *chlamydomonas* centrioles reveals orthologs of ciliary-disease genes. *Curr. Biol.* 15:1090–1098.

Kozminski, K.G., K.A. Johnson, P. Forscher, and J.L. Rosenbaum. 1993. A motility in the eukaryotic flagellum unrelated to flagellar beating. *Proc. Natl. Acad. Sci. USA.* 90:5519–5523.

Kozminski, K.G., P.L. Beech, and J.L. Rosenbaum. 1995. The *Chlamydomonas* kinesin-like protein FLA10 is involved in motility associated with the flagellar membrane. *J. Cell Biol.* 131:1517–1527.

Kroll, E.S., K.M. Hyland, P. Hieter, and J.J. Li. 1996. Establishing genetic interactions by a synthetic dosage lethality phenotype. *Genetics.* 143:95–102.

Lin, F., T. Hiesberger, K. Cordes, A.M. Sinclair, L.S. Goldstein, S. Somlo, and P. Igarashi. 2003. Kidney-specific inactivation of the KIF3A subunit of kinesin-II inhibits renal ciliogenesis and produces polycystic kidney disease. *Proc. Natl. Acad. Sci. USA.* 100:5286–5291.

Liu, K.S., and P.W. Sternberg. 1995. Sensory regulation of male mating behavior in *Caenorhabditis elegans. Neuron.* 14:79–89.

Lucker, B.F., R.H. Behal, H. Qin, L.C. Siron, W.D. Taggart, J.L. Rosenbaum, and D.G. Cole. 2005. Characterization of the intraflagellar transport complex B core: direct interaction of the IFT81 and IFT74/72 subunits. *J. Biol. Chem.* 280:27688–27696.

Marshall, W.F., H. Qin, M. Rodrigo Brenni, and J.L. Rosenbaum. 2005. Flagellar length control system: testing a simple model based on intraflagellar transport and turnover. *Mol. Biol. Cell.* 16:270–278.

Marszalek, J.R., X. Liu, E.A. Roberts, D. Chui, J.D. Marth, D.S. Williams, and L.S. Goldstein. 2000. Genetic evidence for selective transport of opsin and arrestin by kinesin-II in mammalian photoreceptors. *Cell.* 102:175–187.

McGrath, J., S. Somlo, S. Makova, X. Tian, and M. Brueckner. 2003. Two populations of node monocilia initiate left-right asymmetry in the mouse. *Cell.* 114:61–73.

Measday, V., K. Baetz, J. Guzzo, K. Yuen, T. Kwok, B. Sheikh, H. Ding, R. Ueta, T. Hoac, B. Cheng, et al. 2005. Systematic yeast synthetic lethal and synthetic dosage lethal screens identify genes required for chromosome segregation. *Proc. Natl. Acad. Sci. USA.* 102:13956–13961.

Mokrzan, E.M., J.S. Lewis, and K. Mykytyn. 2007. Differences in renal tubule primary cilia length in a mouse model of Bardet-Biedl syndrome. *Nephron Exp. Nephrol.* 106:e88–e96.

Mollet, G., R. Salomon, O. Gribouval, F. Silbermann, D. Bacq, G. Landthaler, D. Milford, A. Nayir, G. Rizzoni, C. Antignac, and S. Saunier. 2002. The gene mutated in juvenile nephronophthisis type 4 encodes a novel protein that interacts with nephrocystin. *Nat. Genet.* 32:300–305.

Mollet, G., F. Silbermann, M. Delous, R. Salomon, C. Antignac, and S. Saunier. 2005. Characterization of the nephrocystin/nephrocystin-4 complex and subcellular localization of nephrocystin-4 to primary cilia and centrosomes. *Hum. Mol. Genet.* 14:645–656.

Mukhopadhyay, S., Y. Lu, H. Qin, A. Lanjuin, S. Shaham, and P. Sengupta. 2007. Distinct IFT mechanisms contribute to the generation of ciliary structural diversity in *C. elegans. EMBO J.* 26:2966–2980.

Nachury, M.V., A.V. Loktev, Q. Zhang, C.J. Westlake, J. Peranen, A. Merdes, D.C. Slusarski, R.H. Scheller, J.F. Bazan, V.C. Sheffield, and P.K. Jackson. 2007. A core complex of BBS proteins cooperates with the GTPase Rab8 to promote ciliary membrane biogenesis. *Cell.* 129:1201–1213.

Nurnberger, J., A. Kribben, A. Opazo Saez, G. Heusch, T. Philipp, and C.L. Phillips. 2004. The Invs gene encodes a microtubule-associated protein. *J. Am. Soc. Nephrol.* 15:1700–1710.

Olbrich, H., M. Fliegauf, J. Hoefele, A. Kispert, E. Otto, A. Volz, M.T. Wolf, G. Sasmaz, U. Trauer, R. Reinhardt, et al. 2003. Mutations in a novel gene, NPHP3, cause adolescent nephronophthisis, tapeto-retinal degeneration and hepatic fibrosis. *Nat. Genet.* 34:455–459.

Orozco, J.T., K.P. Wedaman, D. Signor, H. Brown, L. Rose, and J.M. Scholey. 1999. Movement of motor and cargo along cilia. *Nature.* 398:674.

Otto, E.A., B. Schermer, T. Obara, J.F. O'Toole, K.S. Hiller, A.M. Mueller, R.G. Ruf, J. Hoefele, F. Beekmann, D. Landau, et al. 2003. Mutations in INVS encoding inversin cause nephronophthisis type 2, linking renal cystic disease to the function of primary cilia and left-right axis determination. *Nat. Genet.* 34:413–420.

Otto, E.A., B. Loeys, H. Khanna, J. Hellemans, R. Sudbrak, S. Fan, U. Muerb, J.F. O'Toole, J. Helou, M. Attanasio, et al. 2005. Nephrocystin-5, a ciliary IQ domain protein, is mutated in Senior-Loken syndrome and interacts with RPGR and calmodulin. *Nat. Genet.* 37:282–288.

Otto, E.A., M.L. Trapp, U.T. Schultheiss, J. Helou, L.M. Quarmby, and F. Hildebrandt. 2008. NEK8 mutations affect ciliary and centrosomal localization and may cause nephronophthisis. *J. Am. Soc. Nephrol.* In press.

Ou, G., O.E. Blacque, J.J. Snow, M.R. Leroux, and J.M. Scholey. 2005. Functional coordination of intraflagellar transport motors. *Nature.* 436:583–587.

Ou, G., M. Koga, O.E. Blacque, T. Murayama, Y. Ohshima, J.C. Schafer, C. Li, B.K. Yoder, M.R. Leroux, and J.M. Scholey. 2007. Sensory ciliogenesis in *Caenorhabditis elegans*: assignment of IFT components into distinct modules based on transport and phenotypic profiles. *Mol. Biol. Cell.* 18:1554–1569.

Pan, X., G. Ou, G. Civelekoglu-Scholey, O.E. Blacque, N.F. Endres, L. Tao, A. Mogilner, M.R. Leroux, R.D. Vale, and J.M. Scholey. 2006. Mechanism of transport of IFT particles in *C. elegans* cilia by the concerted action of kinesin-II and OSM-3 motors. *J. Cell Biol.* 174:1035–1045.

Parisi, M.A., C.L. Bennett, M.L. Eckert, W.B. Dobyns, J.G. Gleeson, D.W. Shaw, R. McDonald, A. Eddy, P.F. Chance, and I.A. Glass. 2004. The NPHP1 gene deletion associated with juvenile nephronophthisis is present in a subset of individuals with Joubert syndrome. *Am. J. Hum. Genet.* 75:82–91.

Pathak, N., T. Obara, S. Mangos, Y. Liu, and I.A. Drummond. 2007. The zebrafish fleer gene encodes an essential regulator of cilia tubulin polyglutamylation. *Mol. Biol. Cell.* 18:4353–4364.

Pazour, G.J., and J.L. Rosenbaum. 2002. Intraflagellar transport and cilia-dependent diseases. *Trends Cell Biol.* 12:551–555.

Pazour, G.J., B.L. Dickert, and G.B. Witman. 1999. The DHC1b (DHC2) isoform of cytoplasmic dynein is required for flagellar assembly. *J. Cell Biol.* 144:473–481.

Pazour, G.J., B.L. Dickert, Y. Vucica, E.S. Seeley, J.L. Rosenbaum, G.B. Witman, and D.G. Cole. 2000. *Chlamydomonas* IFT88 and its mouse homologue, polycystic kidney disease gene tg737, are required for assembly of cilia and flagella. *J. Cell Biol.* 151:709–718.

Pazour, G.J., S.A. Baker, J.A. Deane, D.G. Cole, B.L. Dickert, J.L. Rosenbaum, G.B. Witman, and J.C. Besharse. 2002. The intraflagellar transport protein, IFT88, is essential for vertebrate photoreceptor assembly and maintenance. *J. Cell Biol.* 157:103–113.

Perkins, L.A., E.M. Hedgecock, J.N. Thomson, and J.G. Culotti. 1986. Mutant sensory cilia in the nematode *Caenorhabditis elegans. Dev. Biol.* 117:456–487.

Praetorius, H.A., and K.R. Spring. 2001. Bending the MDCK cell primary cilium increases intracellular calcium. *J. Membr. Biol.* 184:71–79.

Praetorius, H.A., and K.R. Spring. 2003. The renal cell primary cilium functions as a flow sensor. *Curr. Opin. Nephrol. Hypertens.* 12:517–520.

Qin, H., D.R. Diener, S. Geimer, D.G. Cole, and J.L. Rosenbaum. 2004. Intraflagellar transport (IFT) cargo: IFT transports flagellar precursors to the tip and turnover products to the cell body. *J. Cell Biol.* 164:255–266.

Qin, H., D.T. Burnette, Y.K. Bae, P. Forscher, M.M. Barr, and J.L. Rosenbaum. 2005. Intraflagellar transport is required for the vectorial movement of TRPV channels in the ciliary membrane. *Curr. Biol.* 15:1695–1699.

Redeker, V., N. Levilliers, E. Vinolo, J. Rossier, D. Jaillard, D. Burnette, J. Gaertig, and M.H. Bre. 2005. Mutations of tubulin glycylation sites reveal cross-talk between the C termini of alpha- and beta-tubulin and affect the ciliary matrix in *Tetrahymena. J. Biol. Chem.* 280:596–606.

Ringo, D.L. 1967. The arrangement of subunits in flagellar fibers. *J. Ultrastruct. Res.* 17:266–277.

Roayaie, K., J.G. Crump, A. Sagasti, and C.I. Bargmann. 1998. The G alpha protein ODR-3 mediates olfactory and nociceptive function and controls cilium morphogenesis in *C. elegans* olfactory neurons. *Neuron.* 20:55–67.

Rosenbaum, J.L., and G.B. Witman. 2002. Intraflagellar transport. *Nat. Rev. Mol. Cell Biol.* 3:813–825.

Rostaing, P., R.M. Weimer, E.M. Jorgensen, A. Triller, and J.L. Bessereau. 2004. Preservation of immunoreactivity and fine structure of adult *C. elegans* tissues using high-pressure freezing. *J. Histochem. Cytochem.* 52:1–12.

Sayer, J.A., E.A. Otto, J.F. O'Toole, G. Nurnberg, M.A. Kennedy, C. Becker, H.C. Hennies, J. Helou, M. Attanasio, B.V. Fausett, et al. 2006. The centrosomal protein nephrocystin-6 is mutated in Joubert syndrome and activates transcription factor ATF4. *Nat. Genet.* 38:674–681.

Schermer, B., K. Hopker, H. Omran, C. Ghenoiu, M. Fliegauf, A. Fekete, J. Horvath, M. Kottgen, M. Hackl, S. Zschiedrich, et al. 2005. Phosphorylation by casein kinase 2 induces PACS-1 binding of nephrocystin and targeting to cilia. *EMBO J.* 24:4415–4424.

Scholey, J.M., and K.V. Anderson. 2006. Intraflagellar transport and cilium-based signaling. *Cell.* 125:439–442.

Scholey, J.M., G. Ou, J. Snow, and A. Gunnarson. 2004. Intraflagellar transport motors in *Caenorhabditis elegans* neurons. *Biochem. Soc. Trans.* 32:682–684.

Shakir, M.A., T. Fukushige, H. Yasuda, J. Miwa, and S.S. Siddiqui. 1993. *C. elegans osm-3* gene mediating osmotic avoidance behaviour encodes a kinesin-like protein. *Neuroreport.* 4:891–894.

Signor, D., K.P. Wedaman, L.S. Rose, and J.M. Scholey. 1999. Two heteromeric kinesin complexes in chemosensory neurons and sensory cilia of *Caenorhabditis elegans. Mol. Biol. Cell.* 10:345–360.

Smith, L.A., N.O. Bukanov, H. Husson, R.J. Russo, T.C. Barry, A.L. Taylor, D.R. Beier, and O. Ibraghimov-Beskrovnaya. 2006. Development of polycystic kidney disease in juvenile cystic kidney mice: insights into pathogenesis, ciliary abnormalities, and common features with human disease. *J. Am. Soc. Nephrol.* 17:2821–2831.

Snow, J.J., G. Ou, A.L. Gunnarson, M.R. Walker, H.M. Zhou, I. Brust-Mascher, and J.M. Scholey. 2004. Two anterograde intraflagellar transport motors cooperate to build sensory cilia on *C. elegans* neurons. *Nat. Cell Biol.* 6:1109–1113.

Stephan, A., S. Vaughan, M.K. Shaw, K. Gull, and P.G. McKean. 2007. An essential quality control mechanism at the eukaryotic Basal body prior to intraflagellar transport. *Traffic.* 8:1323–1330.

Stephens, R.E. 2000. Preferential incorporation of tubulin into the junctional region of ciliary outer doublet microtubules: a model for treadmilling by lattice dislocation. *Cell Motil. Cytoskeleton.* 47:130–140.

Sulston, J.E., D.G. Albertson, and J.N. Thomson. 1980. The *Caenorhabditis elegans* male: postembryonic development of nongonadal structures. *Dev. Biol.* 78:542–576.

Tobin, D., D. Madsen, A. Kahn-Kirby, E. Peckol, G. Moulder, R. Barstead, A. Maricq, and C. Bargmann. 2002. Combinatorial expression of TRPV channel proteins defines their sensory functions and subcellular localization in *C. elegans* neurons. *Neuron.* 35:307–318.

Tory, K., T. Lacoste, L. Burglen, V. Moriniere, N. Boddaert, M.A. Macher, B. Llanas, H. Nivet, A. Bensman, P. Niaudet, et al. 2007. High NPHP1 and NPHP6 mutation rate in patients with Joubert syndrome and nephronophthisis: potential epistatic effect of NPHP6 and AHI1 mutations in patients with NPHP1 mutations. *J. Am. Soc. Nephrol.* 18:1566–1575.

Ward, S., N. Thomson, J.G. White, and S. Brenner. 1975. Electron microscopical reconstruction of the anterior sensory anatomy of the nematode *Caenorhabditis elegans. J. Comp. Neurol.* 160:313–338.

Ware, R.W., D. Clark, K. Crossland, and R.L. Russell. 1975. The nerve ring of the nematode *Caenorhabditis elegans*: sensory input and motor output. *J. Comp. Neurol.* 162:71–110.

Weiss, R.L., D.A. Goodenough, and U.W. Goodenough. 1977. Membrane particle arrays associated with the basal body and with contractile vacuole secretion in *Chlamydomonas. J. Cell Biol.* 72:133–143.

Wemmer, K.A., and W.F. Marshall. 2007. Flagellar length control in *Chlamydomonas*-a paradigm for organelle size regulation. *Int. Rev. Cytol.* 260:175–212.

Wheatley, D.N. 1995. Primary cilia in normal and pathological tissues. *Pathobiology.* 63:222–238.

Winkelbauer, M.E., J.C. Schafer, C.J. Haycraft, P. Swoboda, and B.K. Yoder. 2005. The *C. elegans* homologs of nephrocystin-1 and nephrocystin-4 are cilia transition zone proteins involved in chemosensory perception. *J. Cell Sci.* 118:5575–5587.

Wolf, M.T., J. Lee, F. Panther, E.A. Otto, K.L. Guan, and F. Hildebrandt. 2005. Expression and phenotype analysis of the nephrocystin-1 and nephrocystin-4 homologs in *Caenorhabditis elegans. J. Am. Soc. Nephrol.* 16:676–687.

Yoshimura, S., J. Egerer, E. Fuchs, A.K. Haas, and F.A. Barr. 2007. Functional dissection of Rab GTPases involved in primary cilium formation. *J. Cell Biol.* 178:363–369.